Oxidation of Hydroquinones by $[(bpy)_2(py)Ru^{IV}(O)]^{2+}$ and $[(bpy)_2(py)Ru^{III}(OH)]^{2+}$. Proton-Coupled Electron Transfer

Robert A. Binstead, Mark E. McGuire, Angelos Dovletoglou, Won K. Seok, Lee E. Roecker, and Thomas J. Meyer*

Contribution from the Department of Chemistry, University of North Carolina, Chapel Hill, North Carolina 27599-3290. *Received August 8, 1991*

Abstract: The oxidations of hydroquinone, 2-chlorohydroquinone, and 2,6-dichlorohydroquinone by *cis*-$[(bpy)_2(py)Ru^{IV}(O)]^{2+}$ (bpy is 2,2′-bipyridine; py is pyridine) to their corresponding quinones occur in distinct $1e^-$ steps and follow pH dependent rate laws. Within the pH range 1–8 the rate laws have the form $-d[Ru^{IV}{=}O^{2+}]/dt = [Ru^{IV}{=}O^{2+}][QH_2]\{k_1'[H^+] + k_2 + k_3'[H^+]^{-1}\}$. The term inverse in $[H^+]$ involves the hydroquinone anion, QH^-, as the reductant. For hydroquinone there is a small rate enhancement below pH 3, which arises from the capture of the semiquinone intermediate by $[(bpy)_2(py)Ru^{IV}(O)]^{2+}$, leading to formation of the long-lived ($t_{1/2}$ = 48 s) intermediate, $[(bpy)_2(py)Ru^{II}(p\text{-benzoquinone})]^{2+}$. Below pH 1 there is another source of rate enhancement which appears to arise from a pathway involving the hydroquinone cation, QH_3^+. Fits to the pH dependent kinetic data (T = 20.0 ± 0.2 °C, μ = 0.1 M), under conditions which mask the semiquinone reaction, give k_1' = 1.1 × 10^7 M^{-2} s^{-1}, k_2 = 9.2 × 10^5 M^{-1} s^{-1}, and k_3' = 1.2 × 10^{-2} s^{-1}. The k_2 pathway displays a large H_2O/D_2O kinetic isotope effect of 30 ± 1 at 20 °C, which arises largely from the temperature dependence of the reaction: $\Delta H^{\ddagger}(H_2O)$ = 0.64 ± 0.04 and $\Delta H^{\ddagger}(D_2O)$ = 2.12 ± 0.06 kcal mol^{-1}; $\Delta S^{\ddagger}(H_2O)$ = −29.0 ± 0.1 and $\Delta S^{\ddagger}(D_2O)$ = −30.7 ± 0.2 cal deg^{-1} mol^{-1}. A similar rate law was found for *cis*-$[(bpy)_2(py)Ru^{III}(OH)]^{2+}$ as the oxidant with k_1' = 1.2 × 10^8 M^{-2} s^{-1}, k_2 = 1.1 × 10^6 M^{-1} s^{-1}, and k_3' = 3.7 × 10^{-2} s^{-1}. In strongly acidic solution it is concluded that the oxidation of hydroquinone involves $[(bpy)_2(py)Ru^{III}(OH_2)]^{3+}$ with $k_1 = k_1'$. K_a^{III} = 1.7 × 10^7 M^{-1} s^{-1}. The k_2 pathway displays an H_2O/D_2O kinetic isotope effect of 9.7 ± 0.1 at 20 °C which also arises almost entirely from the temperature dependence of the reaction: $\Delta H^{\ddagger}(H_2O)$ = 1.80 ± 0.05 and $\Delta H^{\ddagger}(D_2O)$ = 3.28 ± 0.03 kcal mol^{-1}; $\Delta S^{\ddagger}(H_2O)$ = −24.7 ± 0.2 and $\Delta S^{\ddagger}(D_2O)$ = −24.2 ± 0.1 cal deg^{-1} mol^{-1}. Both oxidants display a linear H_2O/D_2O mole fraction dependence for k_2 suggesting that the isotope effects for these pH independent pathways involve a single proton transfer. With regard to mechanism, it is concluded that (1) the k_3 pathway for both oxidants occurs by oxidation of the hydroquinone monoanions, (2) the k_1 pathway for Ru(III) involves outer-sphere electron transfer with the aqua ion, $[(bpy)_2(py)Ru^{III}(OH_2)]^{3+}$, as oxidant, (3) the k_2 pathway for both oxidants occurs by *proton-coupled electron transfer* for which, in contrast to H-atom transfer, the electron and proton donor functions of the reducing agent reside at different sites within the molecule.

Introduction

We have utilized polypyridyl–oxo complexes of ruthenium(IV), in particular *cis*-$[(bpy)_2(py)Ru^{IV}(O)]^{2+}$ (py is pyridine; bpy is 2,2′-bipyridine), to probe a number of oxidation mechanisms. These complexes are coordinatively saturated and stable. There is access to both the one-electron Ru(IV/III), Ru(III/II) couples and to the two-electron Ru(IV/II) couple.[1,2] As oxidants they are easily amenable to kinetic studies and to detailed mechanistic investigations based on ^{18}O labeling, pH dependence, H/D isotope effects, and the observation of reaction intermediates.[3-6] By utilizing these mechanistic probes we have concluded, for example, that (1) oxidation of PPh_3 to $O{=}PPh_3$[4a] or of $(CH_3)_2S$ to $(CH_3)_2SO$[4b] occurs by O-atom transfer, (2) oxidation of formate ion to CO_2[5b] or of benzyl alcohol to benzaldehyde[5c] may occur by hydride transfer, and (3) oxidation of hydrogen peroxide to dioxygen, as shown below, occurs by hydrogen atom or proton-coupled electron transfer.[6]

$$(bpy)_2(py)Ru^{IV}{=}O^{2+} + H_2O_2 \rightarrow (bpy)_2(py)Ru^{III}OH^{2+} + HO_2^{\bullet}$$

$$(bpy)_2(py)Ru^{III}OH^{2+} + HO_2^{\bullet} \xrightarrow{\text{rapid}} (bpy)_2(py)Ru^{II}OH_2^{2+} + O_2$$

We report here the results of a detailed study on the oxidation of hydroquinone and some substituted hydroquinones to their corresponding quinones by $[(bpy)_2(py)Ru^{IV}(O)]^{2+}$ or $[(bpy)_2(py)Ru^{III}(OH)]^{2+}$ as oxidants. The mechanism or mechanisms by which the oxidations occur is a particularly interesting point since in the reactions both protons and electrons must be transferred from the reductant to the oxidant. Reasonable mechanisms can be invoked which involve initial proton transfer, initial outer-sphere electron transfer, hydrogen atom transfer, or hydride transfer, all of which are thought to be accessible to the oxidants.

Experimental Section

Materials. High purity deionized water was obtained by passing distilled water through a Nanopure (Barnstead) water purification system. Deuterium oxide (99.9% or 100% D), sulfuric acid-d_2 (99.5% D), sodium deuteroxide (99+% D), and acetonitrile-d_3 (99.6% D) were used as received from Aldrich Chemical Company. Acetonitrile (Baker) was either distilled immediately before use from P_2O_5 under an argon atmosphere, or, in most cases, spectrograde acetonitrile (Burdick & Jackson) was used as received. Hydroquinone (Mallinckrodt), 2-chlorohydroquinone (Eastmak Kodak), 2,6-dichlorohydroquinone (Chemical Dynamics), 2-methylhydroquinone, and 2,3-dimethylhydroquinone (Aldrich) were sublimed before use. Hydroquinone was recrystallized from benzene after purification by sublimation. Sodium phosphate monobasic monohydrate, $NaH_2PO_4{\cdot}H_2O$, sodium phosphate dibasic heptahydrate, $Na_2HPO_4{\cdot}7H_2O$, sodium phosphate tribasic dodecahydrate, $Na_3PO_4{\cdot}12H_2O$, perchloric acid, $HClO_4$, sodium perchlorate, $NaClO_4{\cdot}xH_2O$, sulfuric acid, H_2SO_4, sodium sulfate, Na_2SO_4, and primary standard potassium hydrogen phthalate were used without further purification in the preparation of buffer solutions. Ionic strength was maintained with the use of sodium sulfate. All other materials were reagent grade and were used without additional purification. Prepared by previously reported procedures[1,5b,14b] were $[(bpy)_2(py)Ru^{II}(OH_2)]$-

(1) Moyer, B. A.; Meyer, T. J. *Inorg. Chem.* **1981**, *20*, 436.
(2) (a) Takeuchi, K. J.; Thompson, M. S.; Pipes, D. W.; Meyer, T. J. *Inorg. Chem.* **1984**, *23*, 1845. (b) Dobson, J. C.; Meyer, T. J. *Inorg. Chem.* **1988**, *27*, 3283.
(3) Meyer, T. J. *J. Electrochem. Soc.* **1984**, *131*, 221C.
(4) (a) Moyer, B. A.; Sipe, B. K.; Meyer, T. J. *Inorg. Chem.* **1981**, *20*, 1475. (b) Roecker, L.; Dobson, J. C.; Vining, W. J.; Meyer, T. J. *Inorg. Chem.* **1987**, *26*, 779.
(5) (a) Thompson, M. S.; Meyer, T. J. *J. Am. Chem. Soc.* **1982**, *104*, 4106. (b) Roecker, L.; Meyer, T. J. *J. Am. Chem. Soc.* **1986**, *108*, 4066. (c) Roecker, L.; Meyer, T. J. *J. Am. Chem. Soc.* **1987**, *109*, 746.
(6) (a) Gilbert, J. A.; Gersten, S. W.; Meyer, T. J. *J. Am. Chem. Soc.* **1982**, *104*, 6872. (b) Gilbert, J. A.; Roecker, L.; Meyer, T. J. *Inorg. Chem.* **1987**, *26*, 1126.
(7) (a) Adams, G. E.; Michael, B. D. *Trans. Faraday Soc.* **1967**, *63*, 1171. (b) Willson, R. L. *Trans. Faraday Soc.* **1971**, *67*, 3020. (c) Patel, K. B.; Willson, R. L. *J. Chem. Soc., Faraday Trans. 1* **1973**, *69*, 814. (d) Meisel, D.; Fessenden, R. W. *J. Am. Chem. Soc.* **1976**, *98*, 7505.
(8) Fendler, J. H.; Fendler, E. J. In *The Chemistry Of The Quinoid Compounds*; Patai, S., Ed.; Wiley-Interscience: New York, NY, 1974; Part I, Chapter 10.

0002-7863/92/1514-173$03.00/0

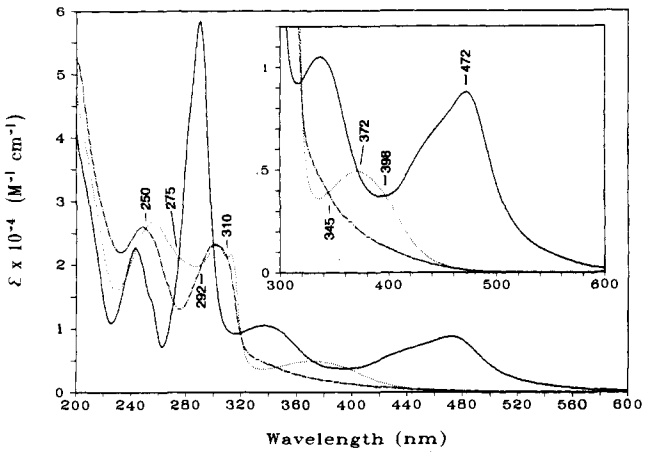

Figure 1. UV–visible spectra of $[(bpy)_2(py)Ru^{II}(OH_2)]^{2+}$ (—), $[(bpy)_2(py)Ru^{III}(OH)]^{2+}$ (···), and $[(bpy)_2(py)Ru^{IV}(O)]^{2+}$ (—·—) in H_2O at T = 22 °C.

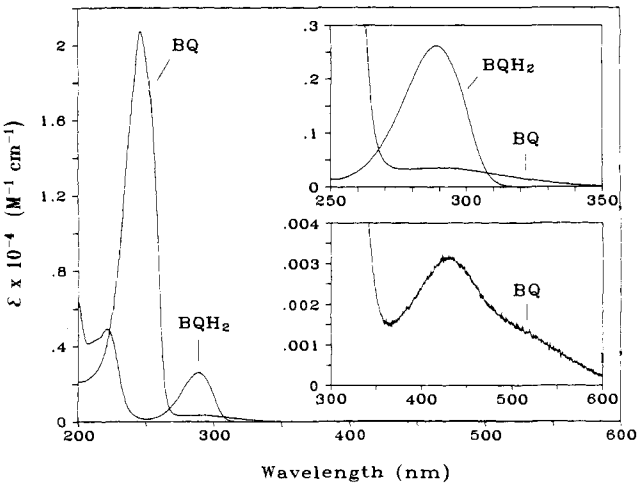

Figure 2. UV–visible spectra of benzoquinone (BQ) and hydroquinone (BQH_2) in H_2O at T = 22 °C.

$(PF_6)_2 \cdot H_2O$, $[(bpy)_2(py)Ru^{IV}(O)](PF_6)_2$, $[(bpy)_2(py)Ru^{IV}(^{18}O)](PF_6)_2$, and their corresponding perchlorate salts.

Instrumentation. Routine UV–visible spectra were recorded on Hewlett Packard 8450A or 8452A diode array spectrophotometers, the latter interfaced with an IBM PC computer. Precision UV–visible spectra were obtained from a modified CARY 14 spectrophotometer interfaced with a Zenith AT type personal computer (OLIS, Jefferson, GA). All manipulations of digitized spectral data were performed using Lab Calc software (Galactic Industries, Salem, NH). IR spectra were obtained on a Nicolet Model 20DX FTIR spectrophotometer as either Nujol mulls or in CH_3CN solution using NaCl plates. ^1H NMR spectra were recorded on an IBM AC 200 spectrometer using CD_3CN (reference vs TMS) or D_2O as solvents.

Stopped-flow kinetics measurements were carried out on two separate systems. Some early experiments were performed by using an Aminco-Morrow stopped-flow apparatus attached to a Beckman DU monochromator, details of which are given elsewhere.[14b] Most of the kinetics experiments were performed by using a Hi-Tech Scientific SF-51 stopped-flow apparatus with fiber-optic coupling to either a Beckman DU or a Harrick rapid scan monochromator. The system was interfaced with a Zenith 158 computer system employing OLIS data acquisition hardware and software. The temperature was controlled to within ±0.2 °C by a Brinkman Lauda K-2/RD water bath circulator.

UV–Visible Spectroscopy. In general, oxidation reactions involving $[(bpy)_2(py)Ru^{IV}(O)]^{2+}$ may proceed in either successive $1e^-$ steps, via $[(bpy)_2(py)Ru^{III}(OH)]^{2+}$, or in a single $2e^-$ step directly to the final product, $[(bpy)_2(py)Ru^{II}(OH_2)]^{2+}$. A distinction between these mechanistic possibilities often can be made spectrophotometrically by following the reactions as a function of wavelength. As shown in Figure 1, there are readily accessible isosbestic points in the spectra (275, 372, 398 nm) which allow the Ru(IV) to Ru(III) reaction to be observed independently of any subsequent reduction from Ru(III) to Ru(II). Similarly, the rate of formation of Ru(II) can be monitored independently (292, 345, 472 nm) in order to determine any difference between the rate of loss of Ru(IV) and the rate of appearance of Ru(II). Such rate differences can be used to distinguish between the $1e^-$ and $2e^-$ pathways provided that the $t_{1/2}$ for the reduction of Ru(IV) is much shorter than the $t_{1/2}$ for comproportionation between Ru(IV) and Ru(II) {$k_{com} = 2.1 \times 10^5$ M^{-1} s^{-1} at T = 25 °C, μ = 0.1 M}[14a,b] which, after an initial $2e^-$ step, gives the same Ru(III) final product as the direct, $1e^-$ pathway. There is no such mechanistic ambiguity in the reactions of $[(bpy)_2(py)Ru^{IV}(O)]^{2+}$ with the hydroquinones since the observed rate constants are much faster than the rate of comproportionation.

The hydroquinones and their corresponding quinone oxidation products have significant UV absorption bands, as shown in Figure 2 for the parent species hydroquinone (BQH_2) and benzoquinone (BQ). Mechanistically, the oxidation of the hydroquinones could proceed via $1e^-$ or $2e^-$ pathways. If the $1e^-$ pathway dominates the reaction, then the formation of the quinone product most likely will proceed via disproportionation of the semiquinone intermediate ($k_{disp} = 1.1 \times 10^9$ M^{-1} s^{-1} for $BQH^{\bullet}$)[7a,8] rather than via direct oxidation by the remaining Ru(IV) or Ru(III). Therefore, the rate of appearance of the quinone product may differ from that of $[(bpy)_2(py)Ru^{II}(OH_2)]^{2+}$. Since the hydroquinone and quinone species are virtually colorless above 380 nm, most of the kinetics measurements have been performed at 398 and 472 nm in order to avoid interference from the rate of appearance of the quinone products. Although the semiquinone species are expected to absorb strongly in the 350–450-nm region,[7a–d,8] their concentrations throughout the reactions are expected to be so small that they should not interfere with the kinetics measurements. Indeed, rapid scan stopped-flow measurements for the Ru(IV) oxidation of hydroquinone revealed no spectroscopic evidence of the semiquinone species. The time evolution of the spectra closely followed that expected from the static spectra presented in Figure 1.

Kinetic Measurements. The oxidations of the hydroquinones by $[(bpy)_2(py)Ru^{IV}(O)]^{2+}$ were studied at 20 °C in neat CH_3CN and H_2O solutions as well as in a variety of aqueous buffer solutions. In the case of hydroquinone the study was extended to include measurements in D_2O and H_2O/D_2O mixtures (pD 4.5). Kinetic data were obtained under pseudo-first-order conditions with at least a 5-fold excess of the hydroquinones. In a typical stopped-flow experiment a 1×10^{-4} M solution of the hydroquinone was mixed with a 2×10^{-5} M solution of the Ru(IV) complex. Under these conditions the observed rate was so fast that 30–50% of the absorbance trace was lost in the mixing time of the apparatus. Thus, the observed portion of the reaction was usually obtained with about a 10-fold excess of the hydroquinone. The rapid reduction of Ru(IV) was monitored at both 398 and 472 nm, though other wavelengths were often used as well for comparison (vide supra). The pH range investigated at μ = 0.1 M was limited at high pH by the rapidity of the reactions: hydroquinone (pH 1–8), 2-chlorohydroquinone (pH 1–7), and 2,6-dichlorohydroquinone (pH 1–5.6). Since the reactions were found to be independent of ionic strength, studies with hydroquinone were extended to pH 0.16 in order to characterize an acid-dependent pathway. Solutions of $[(bpy)_2(py)Ru^{IV}(O)]^{2+}$ were not always stable in the buffer solutions for long periods. This problem was circumvented by mixing the Ru(IV) complex in pure H_2O with hydroquinone in a μ = 0.2 M buffer solution. In general, solutions of the hydroquinones were prepared freshly for each run and subjected to minimal light exposure. Above pH 7, solutions of both the oxidant and reductant were prepared under argon or nitrogen atmospheres and transferred to the stopped-flow apparatus using inert atmosphere techniques to prevent aerial oxidation of the hydroquinone.

The kinetics of the oxidation of hydroquinone by $[(bpy)_2(py)Ru^{III}(OH)]^{2+}$ in aqueous solution were also followed at 20 °C within the pH range 1–7 (μ = 0.1 M), as well as in D_2O and H_2O/D_2O mixtures (pD 4.5). In this case the measurements were made in the presence of excess $[(bpy)_2(py)Ru^{II}(OH_2)]^{2+}$ in order to avoid having appreciable amounts of Ru(IV) present in the oxidant solution due to disproportionation of $[(bpy)_2(py)Ru^{III}(OH)]^{2+}$. Solutions of Ru(III)/Ru(II) were prepared

(9) Perrin, D. D.; Depsey, B. *Buffers for pH and Metal Ion Control*; Science Paperbacks, Chapman and Hall: London, U.K., 1974.
(10) (a) Press, W. H. In *Numerical Recipes. The Art of Scientific Computing*; Cambridge University Press: Cambridge, U.K., 1986. (b) Johnson, K. J. In *Numerical Methods in Chemistry*; Marcel-Dekker: New York, NY, 1980.
(11) Seok, W. K.; Meyer, T. J. *J. Am. Chem. Soc.* **1988**, *110*, 7358.
(12) (a) Brodovitch, J. C.; McAuley, A.; Oswald, T. *Inorg. Chem.* **1982**, *21*, 3442. (b) Bishop, C. A.; Tong, L. K. J. *J. Am. Chem. Soc.* **1965**, *87*, 501.
(13) Pelizzetti, E.; Mentasti, E.; Baiocchi, C. *J. Phys. Chem.* **1976**, *80*, 2979.
(14) (a) Binstead, R. A.; Moyer, B. A.; Samuels, G. J.; Meyer, T. J. *J. Am. Chem. Soc.* **1981**, *103*, 2897. (b) Binstead, R. A.; Meyer, T. J. *J. Am. Chem. Soc.* **1987**, *109*, 3287.

in situ by mixing 1 mol-equiv of Ru(IV) with 2 mol-equiv of Ru(II) just prior to the experiment. Kinetic data were obtained under pseudo-first-order conditions with at least a 10-fold excess of hydroquinone. The observed rate constants for the reduction of Ru(III) to Ru(II) were independent of wavelength so that most kinetic data were collected at 470–472 nm, which is a λ_{max} for the Ru(II) product.

Buffer Solutions. The following media were used for the kinetics measurements in H_2O solutions: $HClO_4$ (pH = 0.16–1.0); $HClO_4/NaClO_4$ (pH = 1.2–1.7); H_2SO_4/Na_2SO_4 or $HClO_4/Na_2SO_4$ (pH = 2.0–2.6); H_3PO_4/NaH_2PO_4 or phthalate/$HClO_4/NaClO_4$ (pH = 2.8–3.0); $HClO_4/Na_2SO_4$ (pH = 3.0–3.3); 0.1 M NaH_2PO_4 (pH = 4.4); NaH_2PO_4/Na_2HPO_4 (pH = 5.0–8.0). In D_2O solutions the following mixtures were used: D_2SO_4 (pD = 0.8–3.0); $D_2SO_4/Na_2SO_4/NaH_2PO_4$ (pD = 4.5–5.2); $NaOD/NaH_2PO_4$ (pD 8.3). The pH of solutions used for kinetic measurements was determined by using a Radiometer Model 62 pH meter and type C glass electrode vs SCE after calibration with standard buffers at 20 °C. For D_2O solutions, pD values were checked by using the pH meter and the relationship $pD = pH_{meas} + 0.4$.[9]

Kinetic Analysis. Nonlinear least-squares fits of the absorbance-time kinetic traces were performed by using a Microsoft QuickBASIC implementation of the Levenberg–Marquardt algorithm.[10a] Two complementary computational methods were used to derive second-order rate constants from the kinetic data. For pseudo-first-order reaction conditions it was possible to fit the data according to eq 1, where A_0 is the initial absorbance, A_∞ is the final absorbance, A_t is the absorbance measured at time t, and k_{obs} is the pseudo-first-order rate constant. In

$$A_t = (A_0 - A_\infty) = \exp(-k_{obs}t) + A_\infty \quad (1)$$

this case the second-order rate constant was obtained by dividing k_{obs} by the midpoint concentration of the species in excess. The latter was estimated from the initial concentration, the measured absorbance change, the cell pathlength (l cm), and the known value of $\Delta\epsilon$ (M^{-1} cm^{-1}) at the wavelength of observation. However, it was generally more convenient to fit the data directly to the full second-order rate equations for equal and unequal concentration conditions according to eqs 2 and 3, respectively, which perform similar scaling within the iterative fitting procedures. These functions provide higher accuracy than the simple exponential fits, particularly with the small pseudo-first-order excesses which had to be used in this work. In the latter case C_A and C_B are the

$$A_t = \frac{(A_0 - A_\infty)}{1 + \frac{(A_0 - A_\infty)}{\Delta\epsilon l}kt} + A_\infty \quad (2)$$

$$A_t = A_0 - \Delta\epsilon l\left[C_A - C_B + \frac{(A_0 - A_\infty)}{\Delta\epsilon l}\right]\left[\frac{\exp[(C_B - C_A)kt] - 1}{\exp[(C_B - C_A)kt] - c_A/c_B}\right] \quad (3)$$

where, $c_B = \frac{(A_0 - A_\infty)}{\Delta\epsilon l}$, $c_A = C_A - C_B + c_B$ and $C_A > C_B$

analytical values of the initial concentrations of species A and B at the time of mixing, while c_A and c_B are the calculated concentrations observed at the instrumental t_{zero} and the other terms remain as defined above. The form of eq 3 provides automatic correction for instrumental dead time based on explicit knowledge of the $\Delta\epsilon$ value. The values of the second-order rate constants obtained from the pseudo-first-order fits (eq 1) were within 1% of those calculated by using the more accurate method in eq 3.

In some cases the initial kinetic processes, monitored at 398 and 472 nm, overlapped the growth and decay of a reaction intermediate which eventually solvolyzed to the final product, $[(bpy)_2(py)Ru^{II}(OH_2)]^{2+}$, on a much slower time scale than observed for the direct reduction steps. It was possible to follow the growth and decay of the intermediate independently at 650 nm (instrumental limit). The successive pseudo-first-order growth and first-order decay processes of the intermediate could be fitted to the sum of two or more exponential functions. The second-order rate constants for the growth kinetics were obtained in a similar manner to that described above for eq 1, after allowance for the amount of the hydroquinone consumed in the preceding steps. The latter was estimated by following the percentage recovery of $[(bpy)_2(py)Ru^{II}(OH_2)]^{2+}$ in each step at 472 nm.

Numerical Simulation of Complex Kinetics. In order to investigate the complex details of the oxidation of hydroquinone by $[(bpy)_2(py)Ru^{IV}(O)]^{2+}$ a number of possible reaction sequences were tested by solving the coupled system of differential rate equations numerically for each model by using a Microsoft QuickBASIC implementation of the fourth-order Runge–Kutta method.[10a,b] These produced product concentration distributions as a function of time which could be compared with experimental observations of the percentage formation of reaction intermediates. The method was also used to assess the effects of parallel, competitive pathways, and sequential Ru(IV) → Ru(III) and Ru(III) → Ru(II) steps on the observed values of the rate constants.

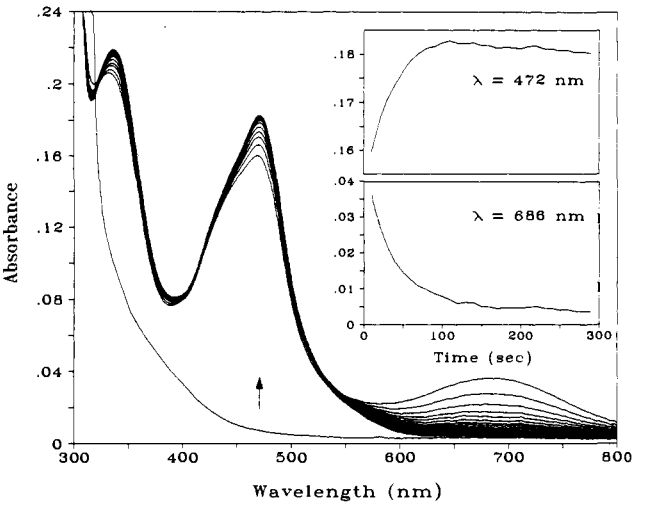

Figure 3. UV–visible spectral changes during the $[(bpy)_2(py)Ru^{IV}(O)]^{2+}$ oxidation of hydroquinone in H_2O at pH = 1 (0.1 M $HClO_4$), T = 20 °C.

Results

Spectral Changes. Rapid scan stopped-flow measurements of the spectral changes accompanying the oxidation of hydroquinone by $[(bpy)_2(py)Ru^{IV}(O)]^{2+}$ in aqueous solution at pH ~ 7 and in CH_3CN revealed that the initially featureless spectrum of the $Ru^{IV}{=}O^{2+}$ complex (Figure 1) changed rapidly to that of $[(bpy)_2(py)Ru^{II}(OH_2)]^{2+}$ (λ_{max} = 472 nm), without evidence of a $Ru^{III}OH^{2+}$ intermediate. In CH_3CN, subsequent spectral changes occur (Figure 1S) consistent with the solvolysis of the initial $[(bpy)_2(py)Ru^{II}(OH_2)]^{2+}$ complex by CH_3CN to yield $[(bpy)_2(py)Ru^{II}(NCCH_3)]^{2+}$ (λ_{max} = 440 nm) as the final product. In acidic, aqueous media the situation becomes much more complex. The rapid, initial reduction of $Ru^{IV}{=}O^{2+}$ leads to $[(bpy)_2(py)Ru^{II}(OH_2)]^{2+}$ in less than 100% yield and is followed by a slower reaction to form an intermediate (λ_{max} = 686 nm) which, as shown in Figure 3, is subsequently transformed very slowly (k_{obs} = 0.02 s^{-1} at pH 1) to the final product $[(bpy)_2(py)Ru^{II}(OH_2)]^{2+}$. This behavior is strikingly similar to our previous observation of the formation and solvolysis of the bound quinone complex, $[(bpy)_2(py)Ru^{II}(benzoquinone)]^{2+}$, during the $Ru^{IV}{=}O^{2+}$ oxidation of phenol.[11] In this case we have been able to extract the spectrum of the intermediate via spectral subtraction (Figure 2S) which clearly demonstrates a Ru(II) MLCT transition to the bpy ligands ($\epsilon \sim 5200$ M^{-1} cm^{-1} at λ_{max} = 442 nm) in addition to the intense MLCT transition to the bound quinone ($\epsilon \sim 8000$ M^{-1} cm^{-1} at λ_{max} = 686 nm).

Product Analysis and Stoichiometry. A spectrophotometric titration showed that $[(bpy)_2(py)Ru^{IV}(O)]^{2+}$ was converted quantitatively into $[(bpy)_2(py)Ru^{II}(OH_2)]^{2+}$ (ϵ = 8800 M^{-1} cm^{-1} at λ_{max} = 472 nm) upon the addition of 1 mol-equiv of hydroquinone in water. The stoichiometry with regard to the organic oxidation product was also established by using ^1H NMR and FTIR spectroscopy in the $\nu_{(C=O)}$ stretching region.[11] A ^1H NMR spectrum obtained after allowing equimolar amounts (15 mM) of $[(bpy)_2(py)Ru^{IV}(O)]^{2+}$ and hydroquinone (BQH_2) to react in 1 mL of CD_3CN showed only the presence of *p*-benzoquinone (BQ) and the acetonitrile complex $[(bpy)_2(py)Ru^{II}(NCCD_3)]^{2+}$.

$$CD_3CN + (bpy)_2(py)Ru^{IV}{=}O^{2+} + BQH_2 \rightarrow H_2O + (bpy)_2(py)Ru^{II}(NCCD_3)^{2+} + BQ \quad (4a)$$

Similar observations were made when the $[(bpy)_2(py)Ru^{III}(OH)]^{2+}$ oxidant was used in 2-fold excess over hydroquinone.

$$CD_3CN + 2(bpy)_2(py)Ru^{III}OH^{2+} + BQH_2 \rightarrow 2H_2O + 2(bpy)_2(py)Ru^{II}(NCCD_3)^{2+} + BQ \quad (4b)$$

Table I. Spectroscopic Data for the Quinone Products from Oxidation of the Corresponding Hydroquinones by $[(bpy)_2(py)Ru^{IV}(O)]^{2+}$ or $[(bpy)_2(py)Ru^{III}(OH)]^{2+}$ in Acetonitrile

		quinone products	
oxidant	reductant QH_2	^1H NMR[a] (ppm vs TMS)	$\nu_{(C=O)}$[b] (cm^{-1})
$[Ru^{IV}=O]^{2+}$	hydroquinone	6.7 (s)	1660, 1674
$[Ru^{IV}=O]^{2+}$	2-chlorohydroquinone	6.6–7.0 (m)	1662, 1684
$[Ru^{IV}=O]^{2+}$	2,6-dichlorohydroquinone	7.2 (s)	1660, 1699
$[Ru^{IV}=O]^{2+}$	2-methylhydroquinone	6.2–6.7 (m)	1662
$[Ru^{IV}=O]^{2+}$	2,3-dimethylhydroquinone	6.7 (s)	1656
$[Ru^{III}OH]^{2+}$	hydroquinone	6.7 (s)	1660, 1674

[a] The yields of the quinone products in CD_3CN were quantitative (±5%). [b] The $\nu_{(C=O)}$ stretching frequencies were measured in CH_3CN solution.

Integration of the ^1H NMR resonances was used to confirm the stoichiometries shown in reactions 4a and 4b. The same stoichiometries were established by UV–visible, ^1H NMR, and FTIR spectroscopy for the reactions between the substituted hydroquinones and $Ru^{IV}=O^{2+}$ in water and acetonitrile. The results of the experiments are summarized in Table I.

The intermediate, $[(bpy)_2(py)Ru^{II}(benzoquinone)]^{2+}$, which was formed during the oxidation of hydroquinone by $Ru^{IV}=O^{2+}$ in H_2O (pH < 6) was not observed when $Ru^{III}OH^{2+}$ was the oxidant. This suggested that ring attack by the oxo complex was required to form the intermediate and that *o*-benzoquinone might also be produced in this reaction pathway. In acidic D_2O solution at pD 1 about 32% of the $[(bpy)_2(py)Ru^{II}(OD_2)]^{2+}$ product was obtained via the Ru^{II}–benzoquinone intermediate. However, the ^1H NMR spectrum of a reaction mixture at pD 1.05 revealed, after solvolysis, that the only oxidation product was *p*-benzoquinone, in contrast to the oxidation of phenol, where 12% of the product was *o*-benzoquinone.[11] Therefore, an ^{18}O tracer study was used to determine whether O-atom transfer occurs during the formation of the intermediate. After oxidation of hydroquinone by $[(bpy)_2(py)Ru^{IV}(^{18}O)](ClO_4)_2$ (from ~98% $H_2{}^{18}O$) in $H_2{}^{16}O$ at pH 1, the *p*-benzoquinone product was extracted with CH_2Cl_2 for analysis. There was no detectable transfer of the ^{18}O label to the *p*-benzoquinone product by using FTIR spectroscopy ($\nu_{(C=^{18}O)}$ = 1646 cm^{-1},[11] $\nu_{(C=^{16}O)}$ = 1660, 1674 cm^{-1} in CH_2Cl_2). This is in marked contrast to the oxidation of phenol where the ^{18}O label appears to be transferred quantitatively to the benzoquinone product.[11] Unfortunately, this result may not be definitive since only 17% of the reaction intermediate was formed at pH 1 in H_2O (cf. 32% in D_2O) so that the FTIR spectrum was masked by the excess *p*-benzoquinone formed in the rapid, direct reduction pathway which, presumably, does not involve ring attack.

Rapid Mixing Experiments To Distinguish between $1e^-$ and $2e^-$ Pathways. The oxidation of hydroquinones by $[(bpy)_2(py)Ru^{IV}(O)]^{2+}$ could occur by initial $1e^-$ or $2e^-$ steps.

$$(bpy)_2(py)Ru^{IV}=O^{2+} + QH_2 \rightarrow (bpy)_2(py)Ru^{III}OH^{2+} + QH^{\bullet} \quad (5a)$$

$$(bpy)_2(py)Ru^{IV}=O^{2+} + QH_2 \rightarrow (bpy)_2(py)Ru^{II}OH^{+} + H^{+} + Q \quad (5b)$$

An initial $1e^-$ step (eq 5a) would be followed most likely by disproportionation of the semiquinone radical, $2QH^{\bullet} \rightarrow QH_2 + Q$ ($k = 1.1 \times 10^9$ M^{-1} s^{-1} for $BQH^{\bullet}$).[7a] However, it is possible that oxidation of $QH^{\bullet}$ by $Ru^{IV}=O^{2+}$, $Ru^{III}OH^{2+}$, or dissolved O_2 could compete with disproportionation under some conditions. In principle, a distinction between the $1e^-$ and $2e^-$ pathways can be made by observing whether the initial product is $[(bpy)_2(py)Ru^{III}(OH)]^{2+}$ or $[(bpy)_2(py)Ru^{II}(OH_2)]^{2+}$. A complication exists in such an analysis since $[(bpy)_2(py)Ru^{II}(OH_2)]^{2+}$, once formed in the presence of $[(bpy)_2(py)Ru^{IV}(O)]^{2+}$, undergoes rapid comproportionation ($k = 2.17 \times 10^5$ M^{-1} s^{-1}, 25 °C, μ = 0.1 M)[14] to give $[(bpy)_2(py)Ru^{III}(OH)]^{2+}$. The ambiguity was absent in this case since the reaction was always observed under conditions where $k_{IV}[Ru(IV)][QH_2] \gg k_{com}[Ru(IV)][Ru(II)]$.

The oxidation of hydroquinone by $[(bpy)_2(py)Ru^{IV}(O)]^{2+}$ in both H_2O and CH_3CN solution displayed wavelength-dependent kinetics, as shown in Figure 4 at pH 5.6 in H_2O (T = 20 °C, μ = 0.1 M, $[QH_2]_0 = 5[Ru]_0$). The rate of disappearance of $[(bpy)_2(py)Ru^{IV}(O)]^{2+}$ (λ_{obs} = 397 nm) was faster than the appearance of $[(bpy)_2(py)Ru^{II}(OH_2)]^{2+}$ (λ_{obs} = 472 nm), consistent with sequential, $1e^-$ reduction steps via the $[(bpy)_2(py)Ru^{III}(OH)]^{2+}$ intermediate. Similar results were obtained at the other isosbestic wavelengths (see Experimental Section). The rate constant for appearance of the $Ru^{II}OH_2{}^{2+}$ complex in this sequential mechanism must be slower than the true rate constant for the Ru(III) → Ru(II) step. The measured rate ratio at pH 5.6 (k_{397}/k_{472} = 1.63) is quite small, suggesting that $k_{III/II}$ is fairly close to $k_{IV/III}$ (k_{397}). A numerical simulation of the sequential reduction mechanism under the pseudo-first-order conditions used in the study gave a rate ratio of 1.59 when $k_{IV/III} = k_{III/II}$. Furthermore, the simulation showed that there would be little buildup of the $Ru^{III}OH^{2+}$ intermediate under such conditions, consistent with the inability of rapid scan stopped-flow measurements to detect its presence. In the limit where $k_{III/II} \gg k_{IV/III}$ the experimental rate constants would be expected to be independent of wavelength. It is clear from these results that only $k_{IV/III}$ can be determined reliably from the kinetics with $Ru^{IV}=O^{2+}$ as the oxidant. Separate studies that use $Ru^{III}OH^{2+}$ as the oxidant are required to determine $k_{III/II}$.

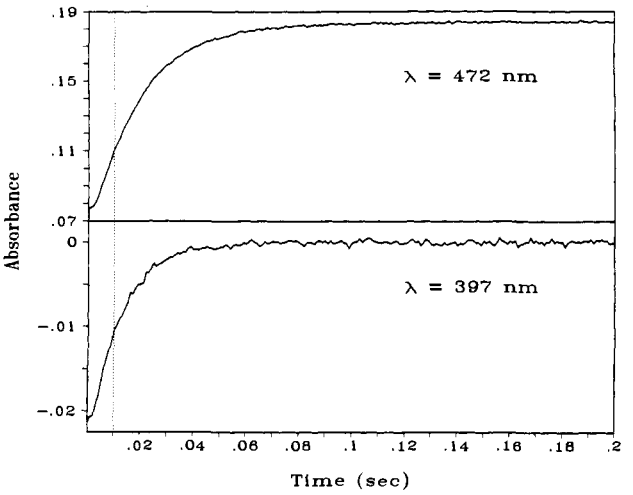

Figure 4. Stopped-flow kinetics traces observed at 397 and 472 nm for the oxidation of hydroquinone (1.07×10^{-4} M) by $[(bpy)_2(py)Ru^{IV}(O)]^{2+}$ (2.09×10^{-5} M) in H_2O at pH = 5.61, μ = 0.1 M, T = 20 °C.

Kinetics: Rate Laws. The oxidation of hydroquinone by $[(bpy)_2(py)Ru^{III}(OH)]^{2+}$ in H_2O was followed under equal concentration and pseudo-first-order conditions with excess hydroquinone. The dependence of k_{obs} on $[QH_2]$ was consistent with the rate law shown in eq 6. This assumes that the rate-determining step was initial $1e^-$ oxidation of QH_2 to the semiquinone ($QH^{\bullet}$), followed by rapid disproportionation, $2QH^{\bullet} \rightarrow QH_2 + Q$ ($k = 1.1 \times 10^9$ M^{-1} s^{-1}).[7a] Under equal concentration conditions the observed kinetics followed a second-order rate law for a 2:1 concentration ratio. This result was reproduced precisely by a numerical simulation of the reaction scheme above. In principle, the $Ru^{III}OH^{2+}$ complex could also react with $QH^{\bullet}$ at a near-to-diffusion-limited rate giving the same final products. It was possible to distinguish between these mechanistic alternatives only when $Ru^{IV}=O^{2+}$ was used as the oxidant.

$$-d[Ru^{III}OH^{2+}]/dt = k_{obs}[Ru^{III}OH^{2+}][QH_2] \quad (6)$$

The kinetics for oxidation of hydroquinone by $[(bpy)_2(py)Ru^{IV}(O)]^{2+}$ in H_2O were studied under equal concentration and pseudo-first-order conditions with an excess of the hydroquinone. Linear plots of k_{obs} vs $[QH_2]$ were obtained over the concentration range 0.024–0.52 mM. The observations were consistent with the rate law shown in eq 7. Under equal concentration conditions

$$-d[Ru^{IV}=O^{2+}]/dt = k_{obs}[Ru^{IV}=O^{2+}][QH_2] \quad (7)$$

the rate of loss of $Ru^{IV}=O^{2+}$ (λ_{obs} = 398 nm) was more complex than observed with $Ru^{III}OH^{2+}$, corresponding to less than 2:1

Table II. Rate Constants for the Oxidation of Hydroquinone by $[(bpy)_2(py)Ru^{IV}(O)]^{2+}$ and $[(bpy)_2(py)Ru^{III}(OH)]^{2+}$ in H_2O at 20 °C, μ = 0.1 M[a]

	$[Ru^{IV}=O]^{2+}$				$[Ru^{III}OH]^{2+}$
pH ± 0.02	%[b] Ru^{II}(quinone)	$k_{IV/III} \times 10^{-6}$[c] ($M^{-1}$ s^{-1})	$k_{IV/II} \times 10^{-6}$[c] (M^{-1} s^{-1})	pH ± 0.02	$k_{III/II} \times 10^{-6}$[c] ($M^{-1}$ s^{-1})
0.16	18.2	1.572 ± 0.064	1.450 ± 0.060		
0.81	17.1	1.397 ± 0.028	1.245 ± 0.020	1.05	7.50 ± 0.31
1.16	19.6	1.324 ± 0.021	1.111 ± 0.010	1.34	4.54 ± 0.19
2.01	17.9	1.238 ± 0.019	0.813 ± 0.004	1.71	2.50 ± 0.04
2.28	16.4	1.148 ± 0.023	0.688 ± 0.006	2.62	1.48 ± 0.04
3.13	11.0	1.033 ± 0.018	0.591 ± 0.004	2.98	1.24 ± 0.05
3.33	10.7	0.950 ± 0.022	0.548 ± 0.005		
4.45	5.0	0.916 ± 0.029	0.565 ± 0.007	4.50	1.12 ± 0.02
5.61	1.3	0.917 ± 0.019	0.563 ± 0.005	5.63	1.10 ± 0.03
6.62	1.0	0.963 ± 0.023	0.630 ± 0.006	6.65	1.27 ± 0.04
				6.98	1.57 ± 0.06
7.60	0.7	1.145 ± 0.042	1.050 ± 0.015	7.59	2.44 ± 0.07
7.92	0.0	1.881 ± 0.053	1.500 ± 0.020		

[a] Ionic strength was maintained constant except for pH < 1. [b] The percent Ru^{II}(quinone) was taken to be (100 − x)%, where x% was the percent of $[(bpy)_2(py)Ru^{II}(OH_2)]^{2+}$ formed prior to growth of the quinone intermediate. [c] $k_{IV/III}$ was calculated from data obtained at 397–398 nm; $k_{IV/II}$ and $k_{III/II}$ were calculated from data at 470–472 nm.

kinetics. However, the rate of growth of $Ru^{II}OH_2^{2+}$ (λ_{obs} = 472 nm) displayed virtually perfect 1:1 kinetic behavior. The results were consistent with a numerical simulation involving initial $1e^-$ oxidation of QH_2 to QH• by both $Ru^{IV}=O^{2+}$ and $Ru^{III}OH^{2+}$ ($k_{IV/III} \sim k_{III/II}$), followed by rapid disproportionation of the semiquinone intermediate. Furthermore, numerical simulations for pseudo-first-order conditions showed that the reaction between $Ru^{III}OH^{2+}$ and QH• could not be competitive with disproportionation since this would result in the appearance of $Ru^{II}OH_2^{2+}$ at almost the same rate as the disappearance of $Ru^{IV}=O^{2+}$. The observation of wavelength dependent kinetics with $Ru^{IV}=O^{2+}$ as the oxidant (vide supra) shows that disproportionation of QH• is the dominant pathway for the appearance of the quinone product.

The oxidation of hydroquinone by $[(bpy)_2(py)Ru^{IV}(O)]^{2+}$ was also studied in CH_3CN under pseudo-first-order conditions at 20 °C, and the results were consistent with the rate law in eq 7. The values obtained for the rate constants were k_{398} = (7.8 ± 0.2) × 10^5 M^{-1} s^{-1} and k_{472} = (4.0 ± 0.4) × 10^5 M^{-1} s^{-1}. These were slightly lower than observed in H_2O at neutral pH (Table II). The larger rate ratio (k_{398}/k_{472} = 1.95) indicates that $k_{III/II} < k_{IV/III}$ in CH_3CN. However, studies with $Ru^{III}OH^{2+}$ as the oxidant were not pursued to confirm this due to the instability of the Ru(III) complex in CH_3CN solution.

Kinetics: pH Dependence. Rate constants for the oxidation of hydroquinone by $Ru^{IV}=O^{2+}$ or $Ru^{III}OH^{2+}$ are collected in Table II. As can be observed from Figure 5, the oxidations are pH dependent. The rate laws remain first-order in $[QH_2]$ and in [oxidant]. However, the reactions are accelerated below pH 2 and above pH 6. For the oxidation of hydroquinone by $[(bpy)_2(py)Ru^{III}(OH)]^{2+}$ the pH dependent rate law takes the form of eq 8, where k_1' and k_3' comprise both rate constants and acid dissociation constants of the reactants. The first pK_a for

$$-d[Ru^{III}OH^{2+}]/dt = [Ru^{III}OH^{2+}][QH_2]\{k_1'[H^+] + k_2 + k_3'[H^+]^{-1}\} \quad (8)$$

$[(bpy)_2(py)Ru^{III}(OH_2)]^{3+}$ has the unusually low value of pK_a^{III} = 0.85 (T = 25 °C, μ = 1 M).[1] At pH values below 0.85 the dominant form of the oxidant is the aqua complex. Therefore, the rate enhancement in highly acidic solution suggests the involvement of $Ru^{III}OH_2^{3+}$ as the oxidant. Furthermore, it can be assumed that the rate enhancement in basic solution arises from the appearance of the hydroquinone anion acting as the reductant ($QH_2 \rightleftharpoons H^+ + QH^-$, pK_a^Q = 9.85).[12b] This results in the rate law taking the form of eq 9. When written in terms of the

$$-d[Ru^{III}]_T/dt = k_1[Ru^{III}OH_2^{3+}][QH_2] + k_2[Ru^{III}OH^{2+}][QH_2] + k_3[Ru^{III}OH^{2+}][QH^-] \quad (9)$$

experimentally measurable quantities, $[Ru^{III}]_T = [Ru^{III}OH_2^{3+}] + [Ru^{III}OH^{2+}]$ and $[Q]_T = [QH_2] + [QH^-]$, this results in the

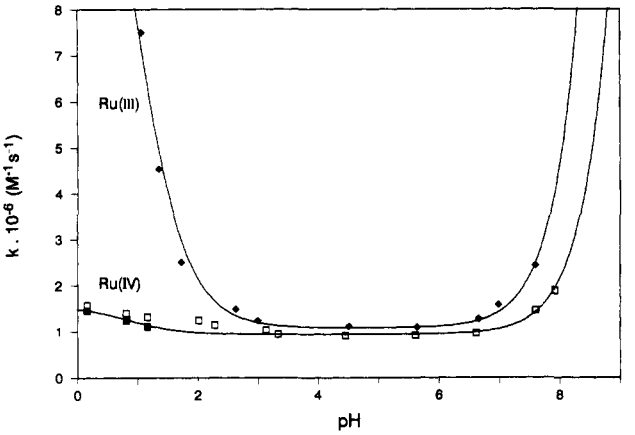

Figure 5. pH dependence of the rate constants for oxidation of hydroquinone by $[(bpy)_2(py)Ru^{IV}(O)]^{2+}$ (□) λ_{obs} = 398 nm, (■) λ_{obs} = 472 nm and by $[(bpy)_2(py)Ru^{III}(OH)]^{2+}$ (♦) λ_{obs} = 472 nm, in H_2O at μ = 0.1 M, T = 20 °C.

form shown in eq 10. Values for k_1, k_2, and k_3 obtained from a fit of the pH dependence of $k_{III/II}$ to eq 10 by using the pK_a values above are listed in Table IV, and the fitted curve is shown in Figure 5.

$$\frac{-d[Ru^{III}]_T}{dt} = \left\{ \frac{k_1}{\left(1 + \frac{K_a^{III}}{[H^+]}\right)\left(1 + \frac{K_a^Q}{[H^+]}\right)} + \frac{k_2}{\left(1 + \frac{[H^+]}{K_a^{III}}\right)\left(1 + \frac{K_a^Q}{[H^+]}\right)} + \frac{k_3}{\left(1 + \frac{[H^+]}{K_a^{III}}\right)\left(1 + \frac{[H^+]}{K_a^Q}\right)} \right\} [Ru^{III}]_T[Q]_T \quad (10)$$

For the oxidation of hydroquinone by $[(bpy)_2(py)Ru^{IV}(O)]^{2+}$ the pH dependent rate law takes the form shown in eq 11, where k_1' and k_3' comprise both rate constants and acid dissociation constants of the reactants. Although the pH dependence appears

$$-d[Ru^{IV}=O^{2+}]/dt = [Ru^{IV}=O^{2+}][QH_2]\{k_1'[H^+] + k_2 + k_3'[H^+]^{-1}\} \quad (11)$$

similar in form to the case of $Ru^{III}OH^{2+}$ as oxidant, the origin of the pH dependence in acidic solution for $Ru^{IV}=O^{2+}$ is much

Table III. Rate Constants for the Oxidation of 2-Chlorohydroquinone and 2,6-Dichlorohydroquinone by $[(bpy)_2(py)Ru^{IV}(O)]^{2+}$ in H_2O at 20 °C, μ = 0.1 M

2-chlorohydroquinone		2,6-dichlorohydroquinone	
pH ± 0.02	$k_{IV/II} \times 10^{-6}$ [a] (M^{-1} s^{-1})	pH ± 0.02	$k_{IV/II} \times 10^{-6}$ [a] (M^{-1} s^{-1})
1.05	1.67 ± 0.12	1.07	3.28 ± 0.27
1.34	1.23 ± 0.07	1.35	3.14 ± 0.16
1.71	1.07 ± 0.06	1.69	3.04 ± 0.20
2.62	0.98 ± 0.05	2.48	3.24 ± 0.19
2.98	0.96 ± 0.04	2.95	2.99 ± 0.24
4.50	1.01 ± 0.05	4.31	3.53 ± 0.23
		4.45	3.97 ± 0.19
5.63	1.64 ± 0.08	5.58	10.8 ± 2.4
6.65	5.77 ± 0.43		
6.98	11.9 ± 1.1		

[a] The reactions were monitored at 470 nm, which is near a λ_{max} for the final product, $[(bpy)_2(py)Ru^{II}(OH_2)]^{2+}$.

more complex. Over the pH range studied, $Ru^{IV}{=}O^{2+}$ and the hydroquinone are the dominant forms of the reactants in solution. There is no spectroscopic or electrochemical evidence for protonation of $[(bpy)_2(py)Ru^{IV}(O)]^{2+}$ even in 1 M acid. However, for hydroquinone there is an accessible protonation equilibrium, $QH_3^+ \rightleftharpoons QH_2 + H^+$ ($pK_a = -0.65 \pm 0.15$ at 25 °C, μ = 0.1 M),[12a] and a deprotonation equilibrium, $QH_2 \rightleftharpoons QH^- + H^+$ ($pK_a = 9.85$ at 25 °C, μ = 1 M).[12b]

Inspection of the rate constants in Table II for the reduction of $Ru^{IV}{=}O^{2+}$ (monitored at 397–398 nm) reveals that there is a small rate enhancement below pH 3. In this same pH domain the formation of the intermediate $[(bpy)_2(py)Ru^{II}(p\text{-benzoquinone})]^{2+}$ reaches a plateau of about 17 ± 1% of the initial [Ru(IV)]. Since the $Ru^{III}OH^{2+}$ oxidant does *not* form this intermediate it follows that $Ru^{IV}{=}O^{2+}$ attack on either QH_2 or QH• is responsible for its appearance. The pH profile for formation of the intermediate (apparent $pK_a = 3.4 \pm 0.1$) is consistent with a reaction in which $Ru^{IV}{=}O^{2+}$ scavenges the semiquinone radical, QH• (pK_a = 4.0–4.1),[7a,b] a feature which will be discussed below in more detail. The scavenging of QH•, to form a Ru^{III}(benzoquinone) intermediate, is responsible for much of the rate enhancement below pH 3.

A more accurate measure of the true rate constant for the $Ru^{IV}{=}O^{2+}$ oxidation of QH_2, $k_{IV/III}$, is available in this circumstance from rate measurements at 472 nm for pH < 1.2, where $k_{III/II} \gg k_{IV/III}$. In this pH domain the net rate constants $k_{IV/II}$ for the appearance of $Ru^{II}OH_2^{2+}$ are slower than observed at 397–398 nm and these reflect the rate of loss of that fraction of $Ru^{IV}{=}O^{2+}$ which has not been attacked by QH•. However, even these rate constants display a pH dependence. The data suggest that for pH < 1 there is a contribution from an additional pathway which is first-order in $[Ru^{IV}{=}O^{2+}]$, $[QH_2]$, and $[H^+]$ to give $[(bpy)_2(py)Ru^{III}(OH_2)]^{3+}$ and QH•. Once formed in this pH domain, $Ru^{III}OH_2^{3+}$ is reduced rapidly by QH_2 (vide supra). Given this interpretation, the rate law for the $Ru^{IV}{=}O^{2+}$ oxidation of QH_2, under conditions which mask the capture of QH• by $Ru^{IV}{=}O^{2+}$, takes the form shown in eq 12. The rate constants

$$\frac{-d[Ru^{IV}]_T}{dt} = \left\{ \frac{k_1}{\left(1 + \frac{K_a^{III}}{[H^+]}\right)\left(1 + \frac{K_a^{Q}}{[H^+]}\right)} + \frac{k_2}{\left(1 + \frac{[H^+]}{K_a^{III}}\right)\left(1 + \frac{K_a^{Q}}{[H^+]}\right)} + \frac{k_3}{\left(1 + \frac{[H^+]}{K_a^{III}}\right)\left(1 + \frac{[H^+]}{K_a^{Q}}\right)} \right\} [Ru^{IV}]_T[Q]_T \quad (12)$$

k_1, k_2, and k_3 which resulted from fitting the values of $k_{IV/II}$ (pH < 1.2) and $k_{IV/III}$ (pH > 4) to eq 12 are listed in Table IV, and the fit is shown in Figure 5. In this case there were sufficient data in acidic solution to allow the value of pK_a^{III} to be an adjustable parameter, and this yielded a value of 0.78 ± 0.15 in close agreement with the measured value of 0.85.[1] The appearance of a rate enhancement centered around pK_a^{III} probably arises from the reaction of QH_3^+ with $Ru^{IV}{=}O^{2+}$ to give either $Ru^{III}OH_2^{3+}$ or $Ru^{III}OH^{2+}$ as the initial product. Further rate enhancement would be expected to appear for pH < 0 where the $[QH_3^+]$ increases.

Table IV. Rate Constants for the Pathways in the pH Dependent Kinetics Model for the Oxidation of the Hydroquinones by $[(bpy)_2(py)Ru^{IV}(O)]^{2+}$ or $[(bpy)_2(py)Ru^{III}(OH)]^{2+}$ at 20 °C

reductant	oxidant	λ_{obs}	k_1, M^{-1} s^{-1}	k_2, M^{-1} s^{-1}	k_3, M^{-1} s^{-1}
hydroquinone	Ru(III)	472	1.68×10^7	1.06×10^6	2.61×10^8
hydroquinone[a]	Ru(IV)	398	1.55×10^6	9.20×10^5	8.61×10^7
hydroquinone	Ru(IV)	472	1.46×10^6	5.75×10^5	8.13×10^7
2-chlorohydroquinone	Ru(IV)	470	2.58×10^6	9.45×10^5	9.10×10^8
2,6-dichlorohydroquinone	Ru(IV)	470	3.31×10^6	3.15×10^6	4.13×10^8

[a] λ_{obs} = 472 nm for pH < 1.2.

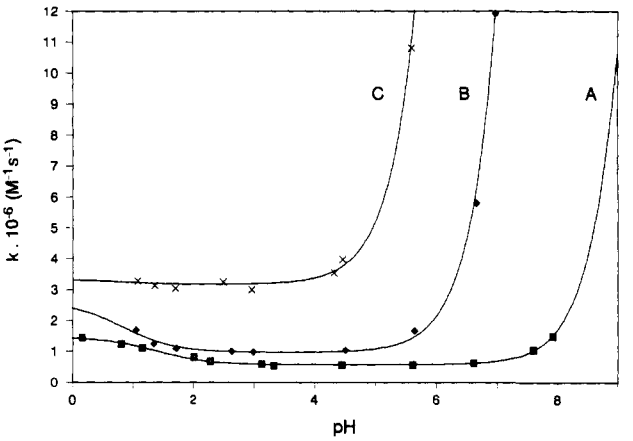

Figure 6. pH dependence of the rate constants for oxidation of (A) hydroquinone (■), (B) 2-chlorohydroquinone (♦), and (C) 2,6-dichlorohydroquinine (×) by $[(bpy)_2(py)Ru^{IV}(O)]^{2+}$ (λ_{obs} = 470 nm) in H_2O at μ = 0.1 M, T = 20 °C.

Similar kinetic behavior was observed for the $Ru^{IV}{=}O^{2+}$ oxidation of 2-chlorohydroquinone and 2,6-dichlorohydroquinone in aqueous media at 20 °C. The pH dependences of the rate constants $k_{IV/II}$, monitored at 470–472 nm, were consistent with the rate law for hydroquinone (eq 12). Independent observations of the Ru(IV) → Ru(III) steps as a function of pH were not made for these reductants. For 2-chlorohydroquinone the rate ratio, k_{397}/k_{470}, was 1.57 at pH 3.0 (T = 22 °C), virtually identical to the result obtained with hydroquinone as the reductant. Unfortunately, the oxidation of 2,6-dichlorohydroquinone proved to be too rapid to obtain a reliable measurement of k_{397} owing to the smaller $\Delta\epsilon$ value at 397 nm. The rate constants obtained for these reductants at 470–472 nm are listed in Table III, and the fits of $k_{IV/II}$ to the rate law in eq 12 are shown in Figure 6. For the substituted hydroquinones the values of pK_a^{III} = 0.85 and pK_a^{Q} = 8.90 (2-chloro) and 7.30 (2,6-dichloro) were used to fit the rate data. For hydroquinone, shown for comparison in Figure 6, it was necessary to allow the value of pK_a^{III} to be an adjustable parameter, giving an effective value of 1.4. This apparent anomaly arises from the onset of rate enhancement from two sources in acidic media: (1) $k_{III/II}$ becomes faster than $k_{IV/III}$ at low pH and (2) $k_{IV/III}$ increases below pH 1. Values for k_1, k_2, and k_3 obtained from the fits by using the pK_a values above are listed in Table IV.

Kinetics: Deuterium Isotope Dependence. In Figure 7 are shown plots of k_X/k_D vs mole fraction D_2O (X_D) for the oxidation of hydroquinone by $[(bpy)_2(py)Ru^{IV}(O)]^{2+}$ or by $[(bpy)_2(py)Ru^{III}(OH)]^{2+}$ in H_2O, D_2O, and H_2O/D_2O mixtures at pH(pD)

Table V. H_2O/D_2O Kinetic Isotope Effects at 20 °C and Activation Parameters (μ = 0.1 M) for Oxidation of Hydroquinone by $[(bpy)_2(py)Ru^{IV}(O)]^{2+}$ or $[(bpy)_2(py)Ru^{III}(OH)]^{2+}$

oxidant	pH	k_H/k_D	$\Delta H^{\ddagger}$ (kcal mol^{-1})	$\Delta S^{\ddagger}$ (cal deg^{-1} mol^{-1})
$Ru^{IV}{=}O^{2+}$ (H_2O)	1.00	28.5 ± 0.6		
	4.45	30.0 ± 1.0	0.64 ± 0.04	−29.0 ± 0.1
	7.92	11.3 ± 0.1		
$Ru^{IV}{=}O^{2+}$ (D_2O)	4.50		2.12 ± 0.06	−30.7 ± 0.2
$Ru^{III}OH^{2+}$ (H_2O)	1.00	1.3 ± 0.1		
	4.45	9.7 ± 0.1	1.80 ± 0.05	−24.7 ± 0.2
	7.53	4.2 ± 0.4		
$Ru^{III}OD^{2+}$ (D_2O)	4.50		3.28 ± 0.03	−24.2 ± 0.1

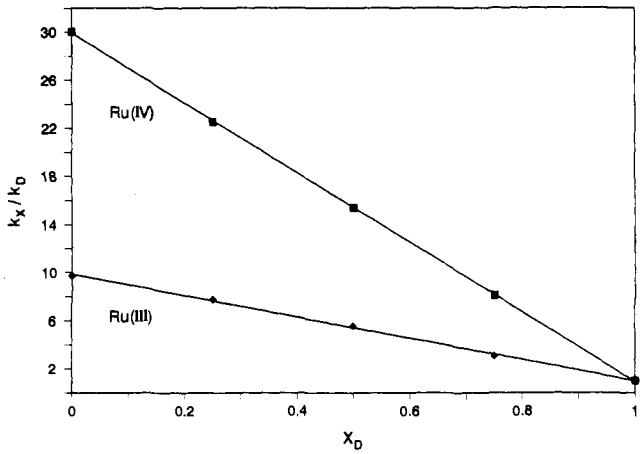

Figure 7. Dependence of the rate constants for oxidation of hydroquinone by $[(bpy)_2(py)Ru^{IV}(O)]^{2+}$ (■) and $[(bpy)_2(py)Ru^{III}(OH)]^{2+}$ (♦) on solvent mole fraction of deuterium (X) at pH/pD = 4.5, μ = 0.1 M, T = 20 °C.

= 4.5, where the acid independent pathway dominates the kinetics. The $k_{(H_2O)}/k_{(D_2O)}$ kinetic isotope effect at 20 °C was also measured at pH = 1.0 and 8.0 for the oxidation of hydroquinone by $Ru^{IV}{=}O^{2+}$ or $Ru^{III}OH^{2+}$, and the results are listed in Table V. At low concentrations of QH_2 with $Ru^{IV}{=}O^{2+}$ as the oxidant the large kinetic isotope effect for the initial redox step resulted in temporal overlap with the growth and decay of the reaction intermediate. Therefore, higher concentrations of QH_2 were used with increasing mole fraction of D_2O so that k_{obs} remained approximately constant and well-separated from this reaction.

Kinetics: Temperature Dependence. Activation parameters for the oxidation of hydroquinone by $[(bpy)_2(py)Ru^{IV}(O)]^{2+}$ or by $[(bpy)_2(py)Ru^{III}(OH)]^{2+}$ were obtained from plots of $\log_e(k/T)$ vs $1/T$, as shown in Figures 8 and 9. The temperature-dependent studies were carried out over the range 5.0–55.0 °C at pH = 4.45, where the acid-independent pathway dominates the kinetics. Activation parameters were obtained in both H_2O and D_2O, and the results are summarized in Table V. The measurements in D_2O had to be made with higher concentrations of hydroquinone than in H_2O so that the observed rate constants were temporally separated from the growth and decay kinetics for the reaction intermediate.

Kinetics: Growth and Decay of the Intermediate. The spectroscopic data presented above provide convincing evidence that $[(bpy)_2(py)Ru^{II}(p\text{-benzoquinone})]^{2+}$ is formed during the oxidation of hydroquinone by $Ru^{IV}{=}O^{2+}$ in acidic media. The pH dependence of the % formation of the intermediate (Table II) displays a plateau level of 17 ± 1% (pH 0–2), then decreases gradually above pH 2, and finally reaches undetectable levels above pH 6. The apparent pK_a^{INT} value of 3.4 ± 0.1 for formation of the intermediate strongly suggests the involvement of the semiquinone radical, QH$^{\bullet}$ (pK_a = 4.0–4.1),[7a,b] rather than QH_2.

In H_2O the kinetics of the growth and decay of the bound $Ru^{II}(p\text{-benzoquinone})^{2+}$ complex were studied at pH 1.00 and pH 4.45 (T = 20 °C, μ = 0.1 M, λ_{obs} = 650 nm) by using hydroquinone in pseudo-first-order excess over $Ru^{IV}{=}O^{2+}$. As shown in Figure 10, the kinetics fit well to a biexponential model (solid

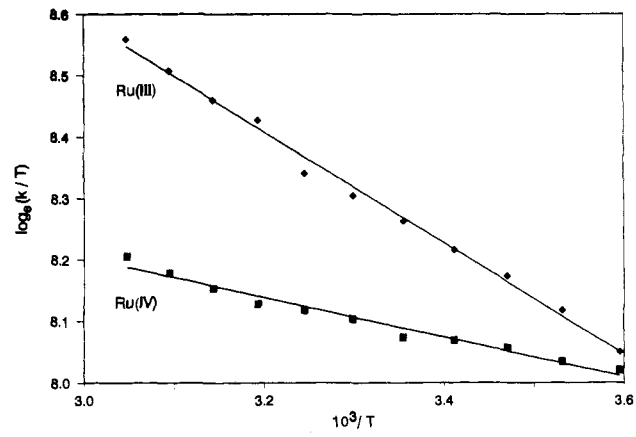

Figure 8. Eyring plots for the temperature dependence of the oxidation of hydroquinone by $[(bpy)_2(py)Ru^{IV}(O)]^{2+}$ (■) and $[(bpy)_2(py)Ru^{III}(OH)]^{2+}$ (♦) in H_2O at pH = 4.45, μ = 0.1 M.

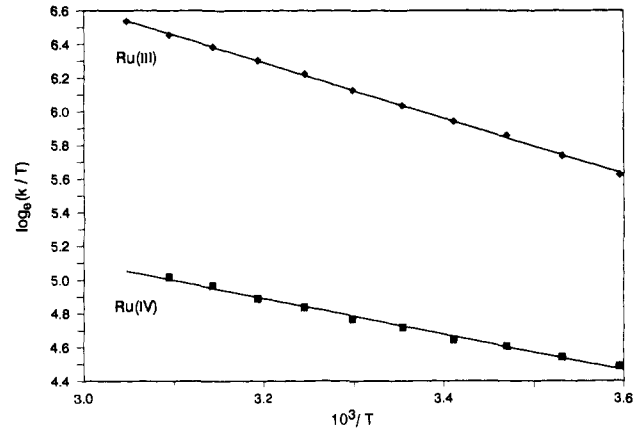

Figure 9. Eyring plots for the temperature dependence of the oxidation of hydroquinone by $[(bpy)_2(py)Ru^{IV}(O)]^{2+}$ (■) and $[(bpy)_2(py)Ru^{III}(OD)]^{2+}$ (♦) in D_2O at pD = 4.5, μ = 0.1 M.

line). The rate of disappearance was found to be independent of the concentrations of both QH_2 and $Ru^{IV}{=}O^{2+}$, with k_{obs}^{D} = 0.022 ± 0.001 s^{-1} at pH 1.00 and k_{obs}^{D} = 0.0504 ± 0.0014 s^{-1} at pH 4.45.

The rate of appearance of the intermediate at pH 1.00 was relatively slow, with k_{obs}^{A} = 0.574 ± 0.007 s^{-1} ($[QH_2]_0$ = 1.028 × 10^{-4} M, $[Ru^{IV}{=}O^{2+}]_0$ = 1.115 × 10^{-5} M). This is almost 500 times slower than the rate of disappearance of $Ru^{IV}{=}O^{2+}$ under these conditions. By inference there must be a preceding intermediate, probably $[(bpy)_2(py)Ru^{III}(p\text{-benzoquinone})]^{3+}$, which is reduced slowly to the spectroscopically observable Ru(II) intermediate by the excess QH_2 reductant. There is some evidence for the Ru(III) intermediate in the kinetics traces at 650 nm. The inset within Figure 10 shows an expanded plot of the growth kinetics, and it is readily observed that there is a rapid preceding kinetic process. When data were obtained for this process on a shorter time scale, the absorbance commenced at zero and then increased with a rate constant, $k_{obs} \sim k_{IV/II}/4$, that was significantly slower than that for the appearance of $Ru^{II}OH_2^{2+}$. The

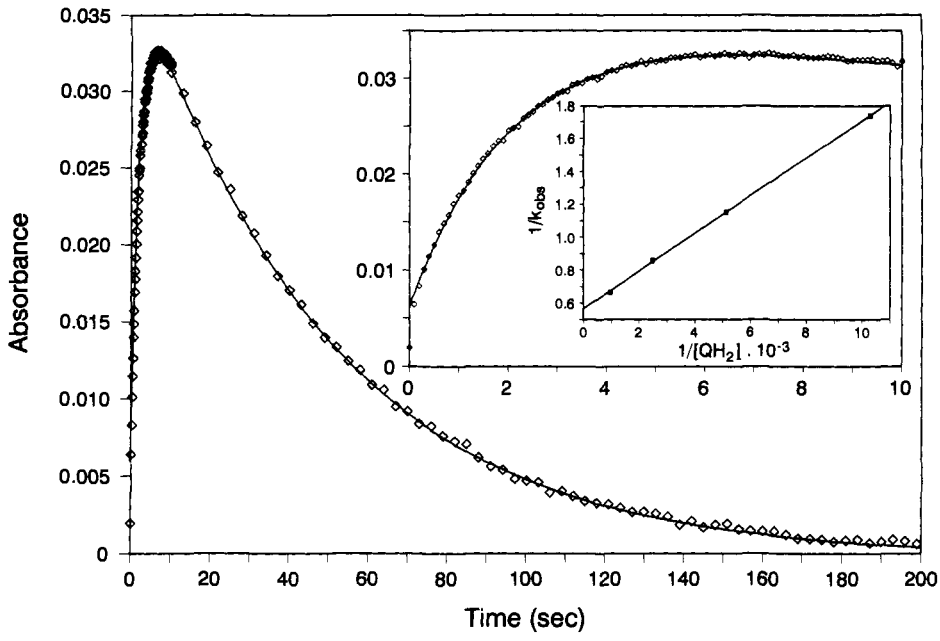

Figure 10. Stopped-flow kinetics trace at 650 nm (◇) and biexponential fit (—) for the growth and decay of the intermediate, $[(bpy)_2(py)Ru^{II}(p\text{-benzoquinone})]^{2+}$, formed during the oxidation of hydroquinone by $[(bpy)_2(py)Ru^{IV}(O)]^{2+}$ in H_2O at pH = 1 ($HClO_4$), T = 20 °C. Inset: inverse–inverse plot of the concentration dependence of k_{obs} for the growth kinetics.

small, rapid increase in absorbance prior to the appearance of $Ru^{II}(p\text{-benzoquinone})^{2+}$ probably arises from the formation of the $Ru^{III}(p\text{-benzoquinone})^{3+}$ precursor from the initial adduct of $Ru^{IV}{=}O^{2+}$ and QH•. Furthermore, $k_{obs}{}^{A}$ was found to depend nonlinearly on $[QH_2]$ over the range 1×10^{-4}–1×10^{-3} M. The behavior was consistent with preassociation of the reactants prior to electron transfer according to the rate law in eq 13, where $[Ru^{III}(Q)]_T$ is the total concentration of the $Ru^{III}(p\text{-benzoquinone})^{3+}$ intermediate, k_{red} is the rate constant for the redox step, and K_A is the equilibrium constant for preassociation. An

$$\frac{-d[Ru^{III}(Q)]_T}{dt} = \frac{k_{red}K_A[QH_2]}{1 + K_A[QH_2]}[Ru^{III}(Q)]_T = k_{obs}[Ru^{III}(Q)]_T \quad (13)$$

inverse–inverse plot of the data according to eq 14 is shown as an inset to Figure 10. A linear least-squares fit of $1/k_{obs}$ vs $1/[QH_2]$ (r_{corr} = 0.9998) yielded values of k_{red} = 1.77 s^{-1} and K_A = 4930 M^{-1}, a remarkably high value corresponding to 33% association at 1×10^{-4} M QH_2. At pH 4.45 the rate of ap-

$$\frac{1}{k_{obs}} = \frac{1}{k_{red}} + \frac{1}{k_{red}K_A[QH_2]} \quad (14)$$

pearance of $Ru^{II}(p\text{-benzoquinone})^{2+}$, $k_{obs}{}^{A}$ = 4.2 ± 0.4 s^{-1}, was 7.3 times faster than at pH 1.00. This is probably a consequence of the greater ease of oxidation of QH_2 with increasing pH since $E°$ for the couple, $Q + 2H^+ + 2e^- \rightleftharpoons QH_2$, is pH dependent.

In D_2O at pD 0.96 (T = 20 °C, μ = 0.1 M) the growth and decay kinetics for the intermediate were similar to the behavior in H_2O. The rate constant for the decay, $k_{obs}{}^{D}$ = 0.025 ± 0.001 s^{-1}, was virtually identical to the value observed in H_2O. Data were collected at only two concentrations, $[QH_2] = 4.00 \times 10^{-4}$ and 1.00×10^{-3} M, for which $k_{obs}{}^{A}$ was 2.06 ± 0.04 and 3.09 ± 0.02 s^{-1}, respectively. These were both approximately twice the values observed in H_2O at the same concentrations. Although there are insufficient data to obtain an accurate measure of the preassociation constant, it does appear that K_A is somewhat smaller than in H_2O solution. At pD 4.5 the rate of appearance of the intermediate was more complex owing to temporal overlap between the rate of reduction of $Ru^{IV}{=}O^{2+}$ by QH_2, for which k_H/k_D = 30, and the growth of the intermediate. The two processes were better resolved at high concentrations of hydroquinone where the second step was rate saturated, although most of the absorbance increase at 650 nm still appeared in the faster step.

Numerical Simulation of Kinetics. The observation of the reaction intermediate, $[(bpy)_2(py)Ru^{II}(p\text{-benzoquinone})]^{2+}$, during the $Ru^{IV}{=}O^{2+}$ oxidation of hydroquinone (BQH_2) and the pH profile for its percent formation provide strong evidence for $Ru^{IV}{=}O^{2+}$ attack on the semiquinone intermediate (BQH•). The sequence of reactions that was used to model the formation of this intermediate is given in eq 15.

$$(bpy)_2(py)Ru^{IV}{=}O^{2+} + BQH_2 \xrightarrow{k_{IV/III}} (bpy)_2(py)Ru^{III}OH^{2+} + BQH^{\bullet} \quad (15a)$$

$$(bpy)_2(py)Ru^{III}OH^{2+} + BQH_2 \xrightarrow{k_{III/II}} (bpy)_2(py)Ru^{II}OH_2{}^{2+} + BQH^{\bullet} \quad (15b)$$

$$(bpy)_2(py)Ru^{IV}{=}O^{2+} + BQH^{\bullet} \xrightarrow{k_{interm}} (bpy)_2(py)Ru^{III}BQ^{3+} + OH^- \quad (15c)$$

$$2BQH^{\bullet} \xrightarrow{k_{disp1}} BQH_2 + BQ \quad (15d)$$

$$BQH^{\bullet} \underset{k_{A^-}}{\overset{k_{HA}}{\rightleftharpoons}} BQ^{\bullet -} + H^+ \quad (15e)$$

$$BQH^{\bullet} + BQ^{\bullet -} + H^+ \xrightarrow{k_{disp2}} BQH_2 + BQ \quad (15f)$$

$$2(bpy)_2(py)Ru^{III}OH^{2+} \underset{k_{com}}{\overset{k_{disp3}}{\rightleftharpoons}} (bpy)_2(py)Ru^{IV}{=}O^{2+} + (bpy)_2(py)Ru^{II}OH_2{}^{2+} \quad (15g)$$

Below pH 2, where BQH• is the dominant form of the semiquinone, eqs 15e and 15f are not significant and can be eliminated from the model. Since $Ru^{IV}{=}O^{2+}$ attack on the semiquinone competes with rapid disproportionation ($k_{disp1} = 1.1 \times 10^9$ M^{-1} s^{-1}),[7a] the value of k_{interm} can be estimated by solving the system of differential rate equations for the reaction model numerically, varying k_{interm} to obtain the experimentally observed product distribution. The results obtained from a simulation under pseudo-first-order conditions ($[BQH_2] = 10^{-4}$ M, [Ru(IV)] = 10^{-5} M) at pH = 1 are shown in Figure 11. The rate constants used in the simulation were the measured values $k_{IV/III} = 9.2 \times 10^5$ M^{-1} s^{-1}, $k_{III/II} = 7.5 \times 10^6$ M^{-1} s^{-1} and the literature values $k_{com} = 2.1 \times 10^5$ M^{-1} s^{-1} and $k_{disp3} = 3 \times 10^3$ M^{-1} s^{-1}.[14] For $k_{interm} = 3.5 \times 10^7$ M^{-1} s^{-1} the simulation gave 17% formation of the $Ru^{III}(benzoquinone)^{3+}$ intermediate, which was the value observed for the Ru(II) form of the intermediate under these conditions.

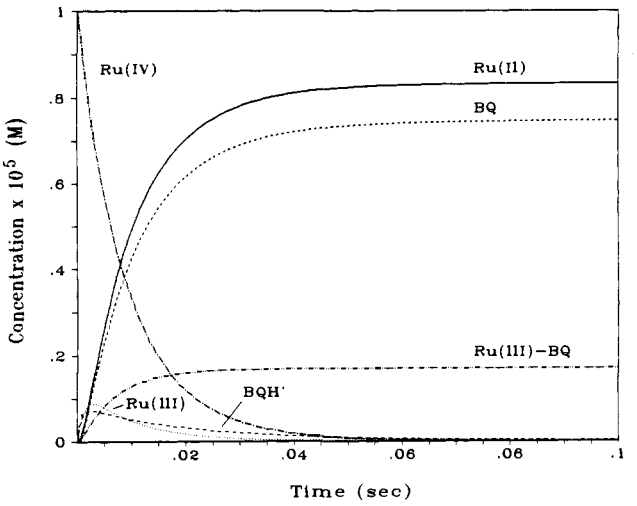

Figure 11. Numerical simulation of the reaction scheme for oxidation of hydroquinone by $[(bpy)_2(py)Ru^{IV}(O)]^{2+}$ in H_2O at pH = 1, μ = 0.1 M, T = 20 °C.

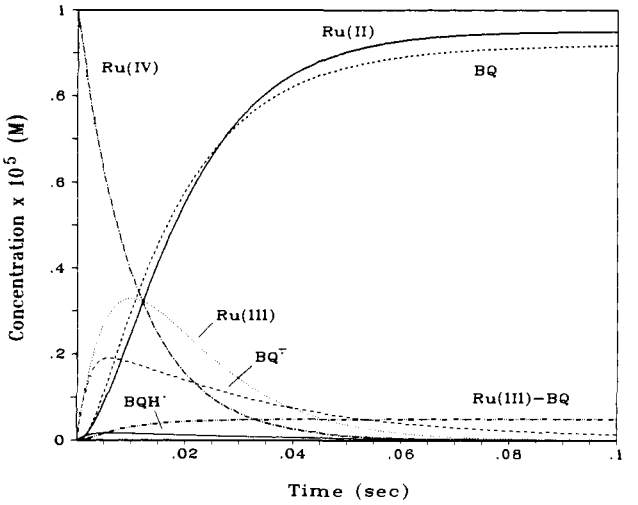

Figure 12. Numerical simulation of the reaction scheme for oxidation of hydroquinone by $[(bpy)_2(py)Ru^{IV}(O)]^{2+}$ in H_2O at pH = 4.5, μ = 0.1 M, T = 20 °C.

At pH 4.5, where about 5% of the intermediate was observed, the pH profile of the semiquinone (eq 15e) was included, together with disproportionation of the semiquinone anion (eq 15f). The additional rate constants used were $k_{III/II} = 1.1 \times 10^6$ M^{-1} s^{-1}, $k_{disp2} = 1.1 \times 10^9$ M^{-1} s^{-1}, $k_{A^-} = 5 \times 10^8$ M^{-1} s^{-1}, and k_{HA} as required by the pK_a of BQH·. The simulation (Figure 12) gave the correct percent formation of the intermediate only if the experimentally determined value of $pK_a = 3.4 \pm 0.1$ was used rather than the literature values (pK_a = 4.0–4.1),[7a,b] obtained from pulse radiolysis experiments.

The intermediate appeared in larger amounts in D_2O solutions due to the large kinetic isotope effect for the oxidation of BQH_2 by $Ru^{IV}{=}O^{2+}$. A numerical simulation for pseudo-first-order conditions at pD = 4.5 ($[BQH_2] = 2 \times 10^{-4}$ M, [Ru(IV)] = 2×10^{-5} M), which used the rate constants $k_{IV/III} = 3.05 \times 10^4$ M^{-1} s^{-1}, $k_{III/II} = 1.12 \times 10^5$ M^{-1} s^{-1}, $k_{com} = 1.30 \times 10^4$ M^{-1} s^{-1}, and $k_{disp3} = 186$ M^{-1} s^{-1},[14] gave the observed value of 13% provided that k_{interm} was reduced to 1.65×10^7 M^{-1} s^{-1}. At pD 1.0, where $k_{III/II} \sim 5.8 \times 10^6$ M^{-1} s^{-1}, the simulation then correctly predicted the observed value of 32–33% formation of the intermediate.

Discussion

Background. In part because of insight that might be gained into related biological redox processes, a number of kinetic studies have been reported on the oxidations of hydroquinone and catechol,

Scheme I

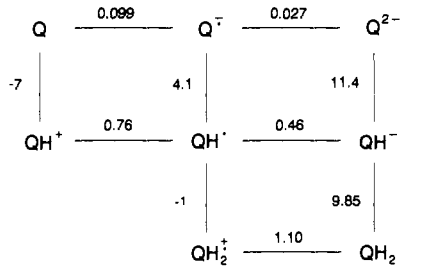

(Q is quinone, QH is semiquinone and QH_2 is hydroquinone)

Scheme II

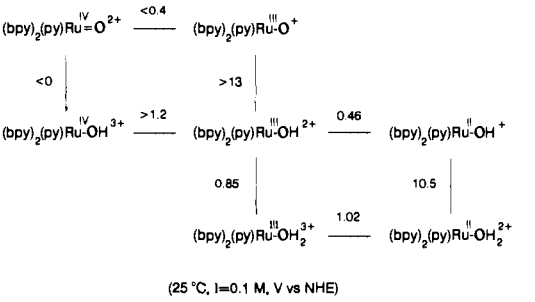

(25 °C, I=0.1 M, V vs NHE)

Scheme III

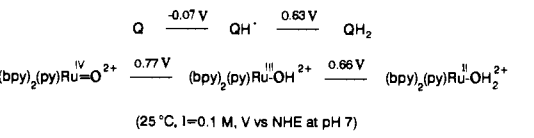

(25 °C, I=0.1 M, V vs NHE at pH 7)

or their derivatives, and of ascorbic acid, which is structurally somewhat related to catechol.

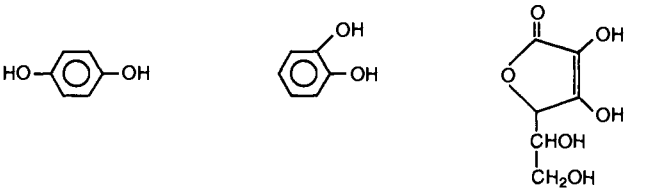

(Hydroquinone) (Catechol) (Ascorbic acid)

For ascorbic acid, evidence has been found with Fe^{3+},[15a] Ce^{IV},[15b] V^V,[16] or IO_4^-[17] as oxidants for either complexation or intermediate formation prior to the redox step. In most reactions studied the mechanisms involve simple outer-sphere electron transfer.[12,13,18-24] One result of the outer-sphere rate studies has been the demonstration of Marcus-type correlations between rate constant and driving force.[12a,13,16b,19,22-25] From these correlations estimates have

(15) (a) Lawrence, G. S.; Ellis, K. J. *J. Chem. Soc., Dalton Trans.* **1972**, 1667. (b) Wells, C. F.; Kuristyn, L. K. *J. Chem. Soc. A* **1965**, 2575.
(16) (a) Kustin, K.; Liu, S. T.; Nicolini, C.; Toppen, D. L. *J. Am. Chem. Soc.* **1974**, *96*, 7410. (b) Kustin, K.; Nicolini, C.; Toppen, D. L. *J. Am. Chem. Soc.* **1974**, *96*, 7416.
(17) (a) Kaiser, E. T.; Weidman, S. W. *Tetrahedron Lett.* **1965**, 497. (b) Weidman, S. W.; Kaiser, E. T. *J. Am. Chem. Soc.* **1966**, *88*, 5820. (c) Mentasti, E.; Pelizzetti, E.; Giraudi, G. *Z. Phys. Chem.* NF **1976**, *100*, 117.
(18) Amjad, Z.; Brodovitch, J. C.; McAuley, A. *Can. J. Chem.* **1977**, *55*, 3581.
(19) Pelizzetti, E.; Mentasti, E.; Pramauro, E. *J. Chem. Soc., Perkin Trans. 2* **1976**, 620.
(20) Pelizzetti, E.; Mentasti, E.; Pramauro, E. *Inorg. Chem.* **1978**, *17*, 1181.
(21) Rickman, R. A.; Sorensen, R. L.; Watkins, K. O.; Davies, G. *Inorg. Chem.* **1977**, *16*, 1570.
(22) Mentasti, E.; Pelizzetti, E.; Baiocchi, C. *J. Chem. Soc., Dalton Trans.* **1971**, 132.
(23) Macartney, D. H.; McAuley, A. *Can. J. Chem.* **1981**, *59*, 132.
(24) McAuley, A.; Oswald, T.; Haines, R. I. *Can. J. Chem.* **1983**, *61*, 1120.

been made of self-exchange rate constants,[19,20,23-25] redox potentials for intermediate one-electron couples such as $QH_2^{\bullet+}/QH_2$,[25] and whether or not outer-sphere electron transfer is accompanied by the loss of a proton in the redox step.[13,22,23] The role of protonation and deprotonation on the electrochemical mechanisms which interconvert quinone and hydroquinone[26] and on their self-exchange reaction[27] have been treated quantitatively by Laviron.

Reduction potentials (vs NHE at 25 °C) for the successive one-electron couples that connect quinone and hydroquinone and pK_a values for the various components are given in Scheme I, as taken from Laviron.[27a] The potential-pK_a data illustrate the profound effect that changes in oxidation state can have on acid–base properties. For example, for $QH_2^{\bullet+}$ compared to QH_2 there is an increase in K_a of nearly 10^{11}. There is an equally profound change in acidity with electron content for the Ru^{IV}/Ru^{III}, Ru^{III}/Ru^{II} couples of the Ru oxidant, as shown by the data in Scheme II.

In either case, changes in acidity with electron content play an important role in dictating the oxidizing or reducing power of the components of the various couples. In a thermodynamic sense, there is always an advantage to forming products which have proton compositions appropriate to the pH of the surrounding medium. This is apparent for the quinone and Ru couples by comparing the potentials in Schemes I and II with those in Scheme III. From these data the strength of $Ru^{IV}{=}O^{2+}$ as a one-electron oxidant is enhanced by >0.4 eV at pH = 7 if $Ru^{III}OH^{2+}$ is the initial product rather than $Ru^{III}O^{+}$. Similarly, the reducing power of QH_2 as a one-electron reductant is enhanced by 0.47 eV if $QH^{\bullet}$ is the initial product rather than $QH_2^{\bullet+}$.

In principle, the impact of proton content on thermodynamics can also dictate the mechanism or mechanisms by which electron transfer occurs. In the oxidation of QH_2 by $[(bpy)_2(py)Ru^{IV}(O)]^{2+}$ five mechanisms that could contribute are (1) initial outer-sphere electron transfer followed by rapid proton transfer

$$(bpy)_2(py)Ru^{IV}{=}O^{2+} + QH_2 \rightarrow (bpy)_2(py)Ru^{III}O^{+} + QH_2^{\bullet+}$$

$$(\Delta G^{\circ\prime} > 16.1 \text{ kcal mol}^{-1})$$

$$(bpy)_2(py)Ru^{III}O^{+} + QH_2^{\bullet+} \xrightarrow{\text{rapid}} (bpy)_2(py)Ru^{III}OH^{2+} + QH^{\bullet} \quad (16a)$$

(2) initial proton transfer followed by electron transfer

$$(bpy)_2(py)Ru^{IV}{=}O^{2+} + QH_2 \rightarrow (bpy)_2(py)Ru^{IV}{=}OH^{3+} + QH^{-}$$

$$(\Delta G^{\circ\prime} > 13.4 \text{ kcal mol}^{-1})$$

$$(bpy)_2(py)Ru^{IV}{=}OH^{3+} + QH^{-} \xrightarrow{\text{rapid}} (bpy)_2(py)Ru^{III}OH^{2+} + QH^{\bullet} \quad (16b)$$

(3) simultaneous one-electron/one-proton transfer

$$(bpy)_2(py)Ru^{IV}{=}O^{2+} + QH_2 \rightarrow (bpy)_2(py)Ru^{III}OH^{2+} + QH^{\bullet} \quad (16c)$$

$$(\Delta G^{\circ\prime} = -3.2 \text{ kcal mol}^{-1})$$

(4) simultaneous two-electron/one-proton transfer

$$(bpy)_2(py)Ru^{IV}{=}O^{2+} + QH_2 \rightarrow (bpy)_2(py)Ru^{II}OH^{+} + QH^{+}$$

$$(\Delta G^{\circ\prime} = +3.8 \text{ kcal mol}^{-1})$$

$$(bpy)_2(py)Ru^{II}OH^{+} + QH^{+} \xrightarrow{\text{rapid}} (bpy)_2(py)Ru^{II}OH_2^{2+} + Q \quad (16d)$$

or (5) simultaneous two-electron/two-proton transfer

$$(bpy)_2(py)Ru^{IV}{=}O^{2+} + QH_2 \rightarrow (bpy)_2(py)Ru^{II}OH_2^{2+} + Q \quad (16e)$$

$$(\Delta G^{\circ\prime} = -20.1 \text{ kcal mol}^{-1})$$

The free energy changes for these and the reactions that follow are at 25 °C, μ = 0.1.

Simultaneous electron/proton transfer utilizes both the full oxidizing strength of $Ru^{IV}{=}O^{2+}$ as a one-electron oxidant and the full one-electron reducing strength of the reductant and is the preferred $1e^{-}$ pathway energetically. However, this pathway is mechanistically more complex and places special demands on the reactants. The oxidizing agent must have acceptor sites for both a proton and an electron. The reducing agent must be capable of donating both an electron and a proton. These criteria are met by the reactants in eq 16, for example, but are not for a simple outer-sphere couple such as $[Fe(bpy)_3]^{3+/2+}$. The two-electron pathways place even more stringent demands on the oxidant. It must be a two-electron acceptor and suffer the consequences of a multiple electron change on the inner-sphere reorganizational energy. Two-electron/two-proton transfer is highly favored energetically because the products are formed with their equilibrium electron and proton contents. However, the activational demands of a simultaneous two-electron/two-proton transfer are severe.

The oxidation of hydroquinone to quinone is highly spontaneous with either $[(bpy)_2(py)Ru^{IV}(O)]^{2+}$ (eq 16e) or $[(bpy)_2(py)Ru^{III}(OH)]^{2+}$ (eq 17) as the oxidant. In either case there is a

$$2(bpy)_2(py)Ru^{III}OH^{2+} + QH_2 \rightarrow 2(bpy)_2(py)Ru^{II}OH_2^{2+} + Q \quad (17)$$

$$(\Delta G^{\circ\prime} = -17.5 \text{ kcal mol}^{-1})$$

requirement for the transfer of two electrons and two protons in the overall reaction. One goal of this study was to establish the mechanisms for these reactions. Does oxidation by $Ru^{III}OH^{2+}$ occur by outer-sphere electron transfer followed by proton transfer? By initial proton transfer followed by electron transfer? By simultaneous electron/proton transfer? Does oxidation by $Ru^{IV}{=}O^{2+}$ occur by initial one-electron or two-electron transfer steps? What is the nature of the proton involvement? What effect does the existence of adjacent forms, e.g., QH^{-} or $[(bpy)_2(py)Ru^{III}(OH_2)]^{3+}$, have on mechanism? If they play a role, new mechanistic pathways will appear which must create a pH dependence.

Oxidation by $[(bpy)_2(py)Ru^{III}(OH)]^{2+}$. From the results of the pH dependent kinetic studies, three separate pathways appear for the oxidation of QH_2 by $[(bpy)_2(py)Ru^{III}(OH)]^{2+}$. Each has its own experimental characteristics and each occurs by a distinct mechanism.

The Pathway $k_2[Ru^{III}OH^{2+}][QH_2]$. In the oxidation of hydroquinone by $Ru^{III}OH^{2+}$, the feature that stands out is the H_2O/D_2O kinetic isotope effect of 9.7 (Table V). From this observation it can be inferred that proton transfer plays an important role in the mechanism. Significant kinetic isotope effects have been observed for other reactions involving this oxidant including H_2O_2 ($k_{(H_2O)}/k_{(D_2O)}$ = 16.2 at 25 °C)[6] and phenol (7.4 at 25 °C).[11] Given the magnitude of the isotope effect and the one-electron character of the oxidant, net H-atom transfer must occur in the redox step to give the semiquinone ($QH^{\bullet}$). This step follows the outer-sphere association of the reactants (eq 18).

$$(bpy)_2(py)Ru^{III}OH^{2+} + QH_2 \rightleftharpoons (bpy)_2(py)Ru^{III}OH^{2+}, QH_2 \quad (18a)$$

$$(bpy)_2(py)Ru^{III}OH^{2+}, QH_2 \rightarrow (bpy)_2(py)Ru^{II}OH_2^{2+}, QH^{\bullet} \quad (18b)$$

$$(bpy)_2(py)Ru^{II}OH_2^{2+}, QH^{\bullet} \rightarrow (bpy)_2(py)Ru^{II}OH_2^{2+} + QH^{\bullet} \quad (18c)$$

$$2QH^{\bullet} \rightarrow QH_2 + Q \quad (18d)$$

$$(bpy)_2(py)Ru^{III}OH^{2+} + QH^{\bullet} \rightarrow (bpy)_2(py)Ru^{II}OH_2^{2+} + Q \quad (18e)$$

(25) Akhtar, M. J.; Haim, A. *Inorg. Chem.* **1988**, *27*, 1608.
(26) Laviron, E. *J. Electroanal. Chem.* **1984**, *164*, 213.
(27) (a) Laviron, E. *J. Electroanal. Chem.* **1984**, *169*, 29. (b) Laviron, E. *J. Electroanal. Chem.* **1986**, *208*, 357.

Table VI. Kinetic Parameters for the Oxidation of Selected Reductants by $[(bpy)_2(py)Ru^{IV}(O)]^{2+}$ or $[(bpy)_2(py)Ru^{III}(OH)]^{2+}$ in H_2O (μ = 0.1 M)

reductant	k (25 °C) (M^{-1} s^{-1})	k_H/k_D (25 °C)	$\Delta H^{\ddagger}$, H_2O ($\Delta H^{\ddagger}$, D_2O) (kcal mol^{-1})	$\Delta S^{\ddagger}$, H_2O ($\Delta S^{\ddagger}$, D_2O) (cal deg^{-1} mol^{-1})
		$Ru^{IV}{=}O^{2+}$ as Oxidant		
$(bpy)_2(py)Ru^{II}(OH_2)^{2+}$ [a]	(2.17 ± 0.03) × 10^5	16.1 ± 0.2	2.3 ± 0.1 (3.9 ± 0.2)	−29.5 ± 0.4 (−29.8 ± 0.8)
H_2O_2 [b]	1.7 ± 0.2	21.6 ± 1.2	6.0 ± 0.3 (9.2 ± 1.2)	−37 ± 3 (−35 ± 4)
hydroquinone [c]	(9.57 ± 0.29) × 10^5	28.7 ± 1.0	0.64 ± 0.04 (2.12 ± 0.06)	−29.0 ± 0.1 (−30.7 ± 0.2)
		$Ru^{III}OH^{2+}$ as Oxidant		
H_2O_2 [b]	(5.44 ± 0.08) × 10^{-2}	16.2 ± 0.7	12 ± 2	−23 ± 5
hydroquinone [c]	(1.16 ± 0.02) × 10^6	9.3 ± 0.1	1.80 ± 0.05 (3.28 ± 0.03)	−24.7 ± 0.2 (−24.2 ± 0.1)

[a] Reference 14b, activation parameters at μ = 3.3 × 10^{-4} M. [b] Reference 6b. [c] This work.

The rate constant for the reaction was independent of whether or not O_2 was present in the solution, which is expected since O_2 does not oxidize QH•.[7c] The semiquinone undergoes disproportionation to the quinone product (eq 18d) at a very rapid rate (k_{disp} = 1.1 × 10^9 M^{-1} s^{-1}).[7a] In order for the semiquinone to be oxidized by $Ru^{III}OH^{2+}$, the rate constant for the reaction (eq 18e) would have to approach the diffusion-controlled limit (k_{diff} = 7 × 10^9 M^{-1} s^{-1}).[27] Measurements under 1:1 concentration conditions displayed kinetic behavior consistent with 2:1 kinetics, in precise agreement with a numerical simulation for initial $1e^-/1\text{-}H^+$ transfer (eq 18b) followed by disproportionation of QH• (eq 18d). Therefore, it appears most likely that the net reaction is as shown in eq 19. The rate-determining step is the initial $1e^-$ oxidation

$$(bpy)_2(py)Ru^{III}OH^{2+} + QH_2 \rightarrow (bpy)_2(py)Ru^{II}OH_2^{2+} + \tfrac{1}{2}QH_2 + \tfrac{1}{2}Q \quad (19)$$

of hydroquinone (eq 18b), and oxidation of QH• by $Ru^{III}OH^{2+}$ does not play an appreciable role. In this case a stoichiometric factor of 2 does not appear in the rate law for the reaction, as it would if eq 18e accounted for the loss of QH•.

For the redox step in eq 18b, possible mechanisms include (1) initial outer-sphere electron transfer followed by rapid proton transfer

$$(bpy)_2(py)Ru^{III}OH^{2+} + QH_2 \rightarrow (bpy)_2(py)Ru^{II}OH^{+} + QH_2^{\bullet+} \quad (20a)$$

$$(\Delta G^{\circ\prime} = 14.8 \text{ kcal mol}^{-1})$$

$$(bpy)_2(py)Ru^{II}OH^{+} + QH_2^{\bullet+} \xrightarrow{\text{rapid}} (bpy)_2(py)Ru^{II}OH_2^{2+} + QH^{\bullet}$$

(2) initial proton transfer followed by outer-sphere electron transfer

$$(bpy)_2(py)Ru^{III}OH^{2+} + QH_2 \rightarrow (bpy)_2(py)Ru^{III}OH_2^{3+} + QH^- \quad (20b)$$

$$(\Delta G^{\circ\prime} = 12.3 \text{ kcal mol}^{-1})$$

$$(bpy)_2(py)Ru^{III}OH_2^{3+} + QH^- \xrightarrow{\text{rapid}} (bpy)_2(py)Ru^{II}OH_2^{2+} + QH^{\bullet}$$

(3) or simultaneous electron-proton transfer

$$(bpy)_2(py)Ru^{III}OH^{2+} + QH_2 \rightarrow (bpy)_2(py)Ru^{II}OH_2^{2+} + QH^{\bullet} \quad (20c)$$

$$(\Delta G^{\circ\prime} = -0.7 \text{ kcal mol}^{-1})$$

The first two can be ruled out based on an energetic argument. For these reactions, the $\Delta G^{\circ\prime}$ values represent minimum free energies of activation, $\Delta G^{\ddagger}$. If it is assumed that their rate constants are of the form $k \geq 10^{13} \exp(-\Delta G^{\circ\prime}/RT)$ (with $\Delta G^{\circ\prime} < \Delta G^{\ddagger}$), the maximum rate constants are 1 × 10^2 M^{-1} s^{-1} for initial electron transfer and 1 × 10^4 M^{-1} s^{-1} for initial proton transfer. Both of these values are considerably less than the experimental value of 1.1 × 10^6 M^{-1} s^{-1}. On the basis of the results of these calculations, the mechanism appears *not* to involve simple electron or proton transfer to give the thermally equilibrated intermediates in eqs 20a,b. Rather, the mechanism must involve the simultaneous transfer of *both* an electron and a proton (eq 20c), which is highly favored energetically over the other two pathways. From the results of the H_2O/D_2O mole fraction study, a single proton is transferred in the redox step.[29]

The Pathway $k_3[Ru^{III}OH^{2+}][QH_2][H^+]^{-1}$. The rate enhancement at higher pH is consistent with the intervention of the hydroquinone monoanion, QH^-, as the reducing agent. With this interpretation, the ratio k_3/k_2 = 250 gives the relative reactivities of QH^- and QH_2 toward $Ru^{III}OH^{2+}$. There is only a limited set of data for the oxidation of QH_2 by other oxidants at higher pH. For ascorbic acid (H_2A) as reductant (K_{a1} = 9.6 × 10^{-5} at 24.8 °C, μ = 1.0 M), accelerations of as high as 10^5 are observed for the oxidation of HA^- compared to H_2A with outer-sphere oxidants.[12,13,18-24] The H_2O/D_2O kinetic isotope effect for this pathway is small, <4.2. From the data at hand, there is no way to distinguish amongst outer-sphere electron transfer, coupled electron-proton transfer, or a combination of the two. Simultaneous electron-proton transfer

$$(bpy)_2(py)Ru^{III}OH^{2+} + QH^- \rightarrow (bpy)_2(py)Ru^{II}OH_2^{2+} + Q^{\bullet-} \quad (21a)$$

$$(\Delta G^{\circ\prime} = -8.6 \text{ kcal mol}^{-1})$$

is favored energetically over outer-sphere electron transfer

$$(bpy)_2(py)Ru^{III}OH^{2+} + QH^- \rightarrow (bpy)_2(py)Ru^{II}OH^{+} + QH^{\bullet} \quad (21b)$$

$$(\Delta G^{\circ\prime} = 0 \text{ kcal mol}^{-1})$$

but to a lesser degree than for the k_2 pathway.

The Pathway $k_1[Ru^{III}OH_2^{3+}][QH_2]$. In strongly acidic solution the dominant form of the Ru(III) oxidant is $[(bpy)_2(py)Ru^{III}(OH_2)]^{3+}$. The rate enhancement in acidic solution is consistent with the oxidation of QH_2 by $[(bpy)_2(py)Ru^{III}(OH_2)]^{3+}$ via a pathway that is first-order in $[(bpy)_2(py)Ru^{III}(OH_2)]^{3+}$ and first-order in QH_2 with k_1(20 °C, μ = 0.1 M) = 1.7 × 10^7 M^{-1} s^{-1}. The H_2O/D_2O kinetic isotope effect (1.3 at 25 °C, μ = 0.1 M) is small and in a range expected for simple outer-sphere electron transfer within an association complex of the reactants (eq 22). The aqua complex is a stronger oxidant than the hydroxo

$$(bpy)_2(py)Ru^{III}OH_2^{3+} + QH_2 \rightleftharpoons (bpy)_2(py)Ru^{III}OH_2^{3+}, QH_2 \quad (22a)$$

$$(bpy)_2(py)Ru^{III}OH_2^{3+}, QH_2 \rightarrow (bpy)_2(py)Ru^{II}OH_2^{2+}, QH_2^{\bullet+} \quad (22b)$$

complex by 0.56 V. This decreases $\Delta G^{\circ\prime}$ for outer-sphere electron transfer from 14.8 (eq 20a) to 1.8 kcal mol^{-1} (eq 23), which

Chart I

oxidant	pathway: $H^+ + QH_2$	pathway: QH_2	pathway: QH^-
$Ru^{III}OH^{2+}$	outer-sphere with $Ru^{III}OH_2^{3+}$ as the oxidant	proton-coupled electron transfer	outer-sphere and/or proton-coupled electron transfer
$Ru^{IV}{=}O^{2+}$	proton-coupled electron transfer with QH_3^+ as the reductant	proton-coupled electron transfer	outer-sphere and/or proton-coupled $1e^-$ or $2e^-$ transfer

explains the enhanced reactivity of this oxidant toward outer-sphere electron transfer. By pH 1 outer-sphere electron transfer,

$$(bpy)_2(py)Ru^{III}OH_2^{3+} + QH_2 \rightarrow (bpy)_2(py)Ru^{II}OH_2^{2+} + QH_2^{\bullet+} \quad (23)$$

$$(\Delta G^{\circ\prime} = 1.8 \text{ kcal mol}^{-1})$$

which is in competition with oxidation of QH_2 by $Ru^{III}OH^{2+}$, dominates the reaction. Because of the large difference in H_2O/D_2O kinetic isotope effects between the two pathways, the involvement of $Ru^{III}OH_2^{3+}$ is important by pH 2 in D_2O.

For other outer-sphere oxidants at $[H^+] > 0.6$ M, rate retardations have been observed.[12,22,24] They have been attributed to protonation of QH_2[12,13,19] and a lowered reactivity of QH_3^+ toward

$$QH_2 + H^+ \rightleftharpoons QH_3^+ \qquad (K_a = 4.5,\ T = 25\ ^\circ\text{C},\ \mu = 1.0\ \text{M})$$

oxidation. Our pH dependent studies were not extended to pH values low enough to observe this effect for $Ru^{III}OH_2^{3+}$.

Oxidation by $[(bpy)_2(py)Ru^{IV}(O)]^{2+}$. For hydroquinone, 2-chlorohydroquinone, and 2,6-dichlorohydroquinone as reductants toward $Ru^{IV}{=}O^{2+}$, the variations in k_{obs} with pH are also consistent with a three term rate law with pathways first-order, zero-order, and inverse-order in $[H^+]$. The mechanistic possibilities increase with $Ru^{IV}{=}O^{2+}$ as oxidant because of its possible access to either $1e^-$ or $2e^-$ pathways.

The Pathway $k_2[Ru^{IV}{=}O^{2+}][QH_2]$. Absorbance vs time traces at pH values where this pathway is dominant show clearly that $[(bpy)_2(py)Ru^{III}(OH)]^{2+}$ is the initial product. This demonstrates that the mechanism involves sequential one-electron-transfer steps. There is a large H_2O/D_2O kinetic isotope effect (30 ± 1) for this pathway, and, from the results of the mole fraction study, a single proton is involved.[29] From the magnitude of the effect it can be inferred that the transfer of a proton from QH_2 to $Ru^{IV}{=}O^{2+}$ within an association complex of the reactants is involved in the redox step. Mechanisms involving initial outer-sphere electron transfer followed by proton transfer (eq 16a) or initial proton transfer followed by electron transfer (eq 16b) can be ruled out on thermodynamic grounds by using the arguments of the previous section. For these reactions, $\Delta G^{\circ\prime} > 16.1$ or > 13.4 kcal mol^{-1}, respectively, and the calculated rate constants are lower than the experimental values by a factor of $>10^3$. Therefore, the mechanism of this reaction also appears to involve simultaneous one-electron/one-proton transfer (eq 16c).

Some interesting qualitative features appear in the variation in k_2 with hydroquinone (Table IV). The $2e^-/1\text{-}H^+$ couples for 2-chlorohydroquinone and 2,6-dichlorohydroquinone are less reducing than hydroquinone by 0.04 and 0.10 V,[30] and yet both are more reactive toward oxidation by $Ru^{IV}{=}O^{2+}$ than is hydroquinone. The absence of any apparent correlation between rate constant and driving force for the $2e^-/1\text{-}H^+$ couples must be a manifestation of the one-electron nature of the redox step.

The Pathway $k_3[Ru^{IV}{=}O^{2+}][QH_2][H^+]^{-1}$. The rate accelerations for the reactions between $Ru^{IV}{=}O^{2+}$ and the hydroquinones as the pH is increased above 4 are also consistent with the hydroquinone anions serving as the reducing agents. As expected, the relative importance of this pathway increases with the acidity of the hydroquinone, as shown in Figure 6.

The H_2O/D_2O kinetic isotope effect of <11.3 is greatly decreased compared to the pathway involving QH_2. The initial redox step could involve (1) outer-sphere electron transfer

$$(bpy)_2(py)Ru^{IV}{=}O^{2+} + QH^- \rightarrow (bpy)_2(py)Ru^{III}O^+ + QH^\bullet \quad (24a)$$

$$(\Delta G^{\circ\prime} > 1.4 \text{ kcal mol}^{-1})$$

(2) simultaneous $1e^-/1\text{-}H^+$ transfer

$$(bpy)_2(py)Ru^{IV}{=}O^{2+} + QH^- \rightarrow (bpy)_2(py)Ru^{III}OH^{2+} + Q^{\bullet-} \quad (24b)$$

$$(\Delta G^{\circ\prime} = -11.1 \text{ kcal mol}^{-1})$$

(3) simultaneous $2e^-/1\text{-}H^+$ transfer

$$(bpy)_2(py)Ru^{IV}{=}O^{2+} + QH^- \rightarrow (bpy)_2(py)Ru^{II}OH^+ + Q \quad (24c)$$

$$(\Delta G^{\circ\prime} = -11.4 \text{ kcal mol}^{-1})$$

or even a combination of the three operating competitively. There is no way to distinguish among them from the present data.

The Pathway $k_1[Ru^{IV}{=}O^{2+}][QH_2][H^+]$. The oxidation of hydroquinone by $Ru^{IV}{=}O^{2+}$ is accelerated in acidic solution (Figure 5), but to a *much* smaller extent than for $Ru^{III}OH_2^{3+}$. Two distinct pathways appear to contribute to the acid dependence. One involves the formation of an intermediate ($\lambda_{max} = 686$ nm), which accounts for $17 \pm 1\%$ of the initial [Ru(IV)] in H_2O at pH 1 and $33 \pm 1\%$ in D_2O at pD 1. The spectral characteristics of this intermediate show that it is the Ru(II) complex, $[(bpy)_2(py)Ru^{II}(benzoquinone)]^{2+}$ ($\lambda_{max} = 675$ nm), which was identified in an earlier study of the oxidation of phenol.[11] In that study the oxidation products were identified as 88% *p*-benzoquinone and 12% *o*-benzoquinone. The small difference in λ_{max} between the two studies probably reflects a difference in product distribution, since only *p*-benzoquinone was observed here as the final product from the oxidation of hydroquinone. Once formed, the quinone complex solvolyzes slowly ($t_{1/2} = 48$ s, $T = 20$ °C) to give free quinone and $[(bpy)_2(py)Ru^{II}(OH_2)]^{2+}$ as the final products.

The kinetic evidence shows that there must be a Ru(III) precursor to the Ru^{II}–quinone^{2+} intermediate. This intermediate is formed via reduction of the Ru(III) precursor by hydroquinone in a relatively slow, pH dependent step. The appearance of the Ru^{II}–quinone^{2+} intermediate tracks the pK_a of the semiquinone ($QH^\bullet$). Since the intermediate is *not* formed when $Ru^{III}OH^{2+}$ is the oxidant, the mechanism must involve the scavenging of $QH^\bullet$ by $Ru^{IV}{=}O^{2+}$, which is in competition with the disproportionation of $QH^\bullet$ (eq 18d). Numerical simulations based on this competition gave $k_{interm} = 3.5 \times 10^7$ M^{-1} s^{-1} for the formation of the Ru(III) precursor, presumably $[(bpy)_2(py)Ru^{III}(p\text{-benzoquinone})]^{3+}$, in H_2O and 1.65×10^7 M^{-1} s^{-1} in D_2O.

The wavelength dependence of the stopped-flow kinetics shows that the remainder of the $Ru^{II}OH_2^{2+}$ product is recovered in rapid, $1e^-/1\text{-}H^+$ steps with a large kinetic isotope effect (28.5 ± 0.6 at pH 1). The kinetic analysis at low pH was complicated by the competition between the pathway $k_2[Ru^{IV}{=}O^{2+}][QH_2]$ and the acid-dependent pathway for loss of $Ru^{IV}{=}O^{2+}$ via capture of $QH^\bullet$. By monitoring the growth of $Ru^{II}OH_2^{2+}$ at 472 nm for pH < 1.2, where $k_{III/II} \gg k_{IV/III}$, it was possible to mask the effects of the pathway involving $QH^\bullet$. Under these conditions there was an additional source of rate enhancement for pH < 1. It was possible

(28) Wells, C. F. *J. Chem. Soc., Faraday Trans.* **1966**, *62*, 2815.
(29) Albery, W. J. In *Proton Transfer Reactions*; Caldin, E., Gold, V., Eds.; Wiley-Interscience: New York, 1975; Chapter 9.
(30) Carlson, B. W.; Miller, L. L. *J. Am. Chem. Soc.* **1985**, *107*, 479.

to fit the pH dependence of the data at 472 nm (Figure 5) by inclusion of the term $k_1[Ru^{IV}{=}O^{2+}][QH_2][H^+]$ in the rate law. This term comprises contributions from the pathways $k_2[Ru^{IV}{=}O^{2+}][QH_2]$ and $k_1''[Ru^{IV}{=}O^{2+}][QH_3^+]$. Since QH• is highly favored over $QH_2^{\bullet+}$ within the pH range studied, the rate enhancement due to the k_1'' pathway appeared to follow the pK_a of $Ru^{III}OH_2^{3+}$. It undergoes rapid reduction by QH_2 in this pH domain to give $Ru^{II}OH_2^{2+}$. A value of $k_1'' \sim 4 \times 10^6$ M^{-1} s^{-1} can be estimated from the fitted value of k_1 (1.5×10^6 M^{-1} s^{-1}) by using the ratio $[QH_2]_0/[Ru^{IV}{=}O^{2+}]_0 \sim 5$ and $k_2 = 9.2 \times 10^5$ M^{-1} s^{-1} with the pK_a values listed above. The same result was obtained from a numerical simulation of the reaction scheme.

Our overall interpretation of the kinetic results in strongly acidic solutions is summarized in Scheme IV. In a mechanistic sense

Scheme IV

(k, M^{-1} s^{-1}, T = 20 °C)

$$(bpy)_2(py)Ru^{IV}{=}O^{2+} + QH_2 \xrightarrow{9.2 \times 10^5} (bpy)_2(py)Ru^{III}OH^{2+} + QH^\bullet$$

$$(bpy)_2(py)Ru^{IV}{=}O^{2+} + QH_3^+ \xrightarrow{4 \times 10^6} (bpy)_2(py)Ru^{III}OH_2^{3+} + QH^\bullet$$

$$(bpy)_2(py)Ru^{III}OH_2^{3+} + QH_2 \xrightarrow{1.7 \times 10^7} (bpy)_2(py)Ru^{II}OH_2^{2+} + QH^\bullet + H^+$$

$$(bpy)_2(py)Ru^{III}OH_2^{3+} + QH^\bullet \rightarrow (bpy)_2(py)Ru^{II}OH_2^{2+} + Q + H^+$$

$$2QH^\bullet \xrightarrow{1.1 \times 10^9} Q + QH_2$$

$$(bpy)_2(py)Ru^{IV}{=}O^{2+} + QH^\bullet \xrightarrow{3.5 \times 10^7} (bpy)_2(py)Ru^{III}(OHQ)^{3+}$$

$$(bpy)_2(py)Ru^{III}(OHQ)^{3+} + H^+ \xrightarrow{\text{rapid}} (bpy)_2(py)Ru^{III}(p\text{-benzoquinone})^{3+} + H_2O$$

$$(bpy)_2(py)Ru^{III}(p\text{-benzoquinone})^{3+} + QH_2 \underset{}{\overset{4930\ M^{-1}}{\rightleftharpoons}} (bpy)_2(py)Ru^{III}(p\text{-benzoquinone})^{3+}, QH_2$$

$$(bpy)_2(py)Ru^{III}(p\text{-benzoquinone})^{3+}, QH_2 \xrightarrow{1.77\ s^{-1}} (bpy)_2(py)Ru^{II}(p\text{-benzoquinone})^{2+} + QH^\bullet + H^+$$

$$(bpy)_2(py)Ru^{II}(p\text{-benzoquinone})^{2+} + H_2O \xrightarrow{0.02\ s^{-1}} (bpy)_2(py)Ru^{II}(OH_2)^{2+} + Q$$

there are some notable reactions in Scheme IV. The appearance of the acid-dependent pathway implies that preprotonation occurs at either QH_2, to give QH_3^+, or at $Ru^{IV}{=}O^{2+}$, to give $[(bpy)_2(py)Ru^{IV}(OH)]^{3+}$. While there is no spectroscopic evidence for the latter, new transitions do appear in the UV spectrum of QH_2 below pH 1. From the large isotope effect observed at pH 1, where the acid-dependent pathway contributes significantly, it can be inferred that this reaction also involves a simultaneous electron/proton transfer mechanism. The apparent capture of QH• by $[(bpy)_2(py)Ru^{IV}(O)]^{2+}$ is also notable. This reaction is remarkably rapid ($k = 3.5 \times 10^7$ M^{-1} s^{-1}) given that it must involve attack on the aromatic ring of the semiquinone radical. This appears to give the quinone bound to Ru(III) initially. Since the quinone complex does not appear as an intermediate past the pK_a of QH•, ring attack must be activated by protonation. This reaction shares some common features with the rapid attack of OH• on the aromatic ring of hydroquinone ($k = 1.2 \times 10^8$ M^{-1} s^{-1}), which has been observed in pulse radiolysis experiments.[7a,8] The latter reaction results in formation of the trihydroxycyclohexadienyl radical, which rapidly eliminates H_2O to give the *p*-hydroxy form of the semiquinone, QH•.[7a,8] Similarly, the $Ru^{IV}{=}O^{2+}$ reaction with QH• leads to the *p*-benzoquinone complex with net elimination of H_2O. The observation of saturation kinetics for the reduction of $[(bpy)_2(py)Ru^{III}(p\text{-benzoquinone})]^{3+}$ by QH_2 shows that a relatively stable (K_A = 4930 M^{-1}) preassociation complex is formed. The origin of this stability may lie in a strong H-bonding interaction between QH_2 and the bound quinone.

Scheme V

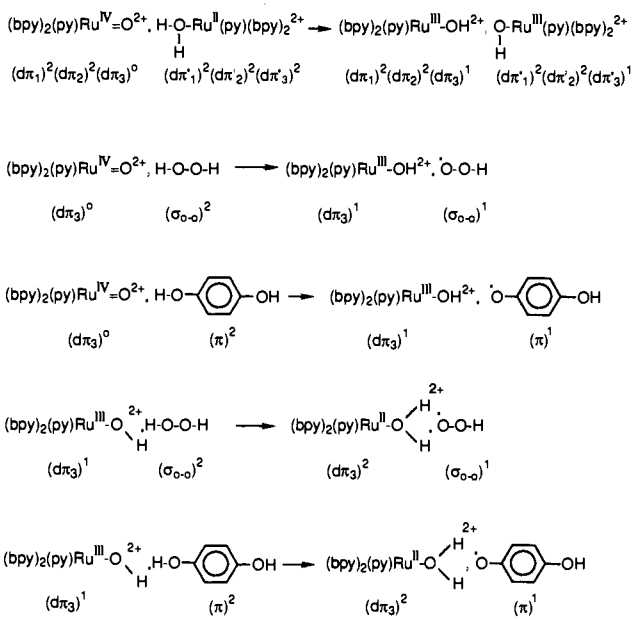

Mechanistic Summary. The conclusions that have been reached concerning mechanisms for the various pathways for both $[(bpy)_2(py)Ru^{IV}(O)]^{2+}$ and $[(bpy)_2(py)Ru^{III}(OH)]^{2+}$ as oxidants are collected and summarized in Chart I.

Proton-Coupled Electron Transfer. The kinetic parameters for the oxidations of $[(bpy)_2(py)Ru^{II}(OH_2)]^{2+}$, H_2O_2, or hydroquinone by $[(bpy)_2(py)Ru^{IV}(O)]^{2+}$ and of H_2O_2 or hydroquinone by $[(bpy)_2(py)Ru^{III}(OH)]^{2+}$ are summarized in Table VI. Although the three reductants are seemingly dissimilar chemically, each has dissociable protons and their reactions have three features in common: (1) Each occurs with a large H_2O/D_2O kinetic isotope effect. Where the data are available from mole fraction studies, it can be inferred that a single proton is transferred in the redox step. (2) The isotope effect resides largely in $\Delta H^\ddagger$ or E_a. (3) The entropies of activation are large and negative and are relatively unaffected by the change in solvent from H_2O to D_2O.

These facts point to mechanistic features in common for the three reductants. From the magnitudes of the H_2O/D_2O kinetic isotope effects and the thermodynamic arguments developed here, the key feature in the mechanism is the occurrence of a simultaneous electron/proton transfer from the reducing agent to $Ru^{IV}{=}O^{2+}$ or to $Ru^{III}OH^{2+}$. The reactions that occur within the association complexes of the reactants for the five reactions are shown in Scheme V. The electronic configurations or redox orbitals of the electron acceptors and electron donors are also indicated for each case. The reactants are shown in orientations within the association complexes which provide a spatial basis for meeting the orbital overlap demands of a simultaneous electron-proton transfer. These particular orientations represent a relatively small sampling of all possible orientations that are accessible to the reactants. They may be stabilized by H-bonding interactions.

In all five reactions, an electron-proton pair is transferred simultaneously from the reductant to the oxidant. For all three reducing agents, the electron- and proton-transfer functions reside at orbitally different sites. Electronic motion away from $Ru^{II}OH_2^{2+}$, H_2O_2, or QH_2 to $Ru^{IV}{=}O^{2+}$ or $Ru^{III}OH^{2+}$ increases the acidity of –OH protons in the donor and increases the basicity of the acceptor. The enhanced acidity at one site and enhanced basicity at the other promotes proton transfer. Taking as the example $[(bpy)_2(py)Ru^{II}(OH_2)]^{2+}$ as reducing agent, electron transfer occurs from a filled $d\pi$ orbital, $d\pi_3$, which is largely Ru(3d) in character. Proton transfer occurs from bound H_2O

via a $\sigma_{(O-H)}$ bond. For H_2O_2 and hydroquinone as reducing agents there are acidic protons in $\sigma_{(O-H)}$ bonds and redox orbitals which are either σ_{O-O} or π in character.

In a simultaneous electron-proton transfer, intramolecular electronic interactions between $\sigma_{(O-H)}$ and the redox orbitals lead to electronic communication between sites and the correlated transfer of both groups to the oxidant. The critical mode is a $\nu_{(O-H)}$ stretch and the motions of the electron and proton are coupled.

The utilization of a simultaneous electron/proton-transfer pathway places special demands on the oxidant as well as the reductant. The oxidant must be capable of accepting *both* an electron and a proton simultaneously. This requirement is met by either $[(bpy)_2(py)Ru^{IV}(O)]^{2+}$ or $[(bpy)_2(py)Ru^{III}(OH)]^{2+}$ as oxidants. These contain both electron and proton *acceptor* capabilities, which are also based on separate sites. The electron is accepted into a vacancy in the $d\pi$ orbitals. The proton is transferred to the O-atom of, what is initially, the oxo group of Ru(IV) or the hydroxo group of Ru(III).

The reactions in Scheme V stand in contrast to the allylic oxidation of olefins[31a] or the oxidations of HCO_2^- or of $PhCH_2OH$ by $[(bpy)_2(py)Ru^{IV}(O)]^{2+}$. In these reactions H_2O/D_2O kinetic isotope effects are negligible, but large C-H/C-D kinetic isotope effects are observed.[5,31] It has been suggested in these cases that the mechanisms involve direct attack on a C-H bond. The C-H bond serves as the source of both electrons and protons. Both are transferred in the redox step.

We propose that there are at least two distinct mechanisms for simultaneous electron/proton transfer. We also propose that one be called *proton-coupled electron transfer*. In this mechanism (Scheme V) the electron and proton donor functions are located at separate sites in the reductant but are transferred simultaneously. It can be anticipated that other examples will be found based on proton transfer from dissociable -NH or -SH bonds. Although the examples studied here involve one-electron transfer, there is also the possibility that proton-coupled two-electron transfer may occur in some reactions. In a second mechanism involving simultaneous electron-proton transfer, the transfer occurs from the same bond. We propose that the term *hydrogen atom transfer* be reserved for this direct transfer of an e^-/H^+ pair from the same bond of the reductant to the oxidant.

(31) (a) Curry, M.; Dobson, J. C.; Stultz, L.; Meyer, T. J., manuscript in preparation. (b) Dobson, J. C.; Seok, W. K.; Meyer, T. J. *Inorg. Chem.* **1986**, *25*, 1514.

Acknowledgment is made to the National Science Foundation for financial assistance from Grant Nos. CHE-8601604 and CHE-8906794 and from the National Institutes of Health under Grant No. 5-RO1-GM32296-06.

Registry No. BQ, 106-51-4; $[(bpy)_2(py)Ru^{IV}(O)]^{2+}$, 67202-43-1; $[(bpy)_2(py)Ru^{III}(OH)]^{2+}$, 75495-07-7; $[(bpy)_2(py)Ru^{II}(OH_2)]^{2+}$, 67202-42-0; $[(bpy)_2(py)Ru^{II}(NCCH)]^{2+}$, 82769-09-3; $[(bpy)_2(py)Ru^{II}$-(benzoquinone)$]^{2+}$, 116374-54-0; titanium, 7440-32-6; hydroquinone, 123-31-9; 2-chlorohydroquinone, 615-67-8; 2,6-dichlorohydroquinone, 20103-10-0; 2-methylhydroquinone, 95-71-6; 2,6-dimethylhydroquinone, 608-43-5; 2-chloro-2,5-cyclohexadiene-1,4-dione, 695-99-8; 2,6-dichloro-2,5-cyclohexadiene-1,4-dione, 697-91-6; 2-methyl-2,5-cyclohexadiene-1,4-dione, 553-97-9; 2,6-dimethyl-2,5-cyclohexadiene-1,4-dione, 526-86-3.

Supplementary Material Available: Figure 1S, showing the solvolysis of the reduction product $[(bpy)_2(py)Ru^{II}(OH_2)]^{2+}$ by CH_3CN, and Figure 2S, showing the spectrum of the reaction intermediate $[(bpy)_2(py)Ru^{II}(p\text{-benzoquinone})]^{2+}$ (2 pages). Ordering information is given on any current masthead page.

Equilibrium between 2-Oxomorpholin-3-yl Radicals and Viologen Radicals. Determination of Reduction Potentials

Robert Patrick Mahoney, Paul A. Fretwell, Samuel H. Demirdji, R. L. Mauldin, III,† Olester Benson, Jr., and Tad H. Koch*

Contribution from the Department of Chemistry and Biochemistry, University of Colorado, Boulder, Colorado 80309-0215. *Received July 5, 1991. Revised Manuscript Received August 22, 1991*

Abstract: Bi(3,5,5-trimethyl-2-oxomorpholin-3-yl) (TM-3 dimer) undergoes bond homolysis to yield 3,5,5-trimethyl-2-oxomorpholin-3-yl (TM-3), which reduces propyldiquat (PDQ^{2+}) to its radical cation PDQ^+. The byproduct is 5,6-dihydro-3,5,5-trimethyl-1,4-oxazin-2-one (**8**). Similarly, bi(5,5-dimethyl-4-ethyl-2-oxomorpholin-3-yl) (DEM-3 dimer) cleaves to 5,5-dimethyl-4-ethyl-2-oxomorpholin-3-yl (DEM-3), which reduces paraquat (PQ^{2+}) to its radical cation PQ^+. The byproduct, 5,5-dimethyl-4-ethyl-3-methoxy-2-oxomorpholine (**10**), results from rapid addition of methanol solvent to the transient 5,6-dihydro-4-ethyl-5,5-dimethyl-1,4-oxazin-2-onium cation (**11**). Concentration versus time data for the respective viologen radical cations together with reduction potentials for the viologens place the reduction potentials for TM-3 dimer and DEM-3 dimer at -0.56 and -0.33 V versus NHE, respectively, in Tris/Tris·H^+ buffered methanol. The kinetics of reduction are analyzed using numerical integration, and the two reducing agents are compared with dithionite.

Introduction

3,5,5-Trimethyl-2-oxomorpholin-3-yl (TM-3) is a persistent carbon radical of the captodative[1] or merostablized class,[2] which shows one-electron redox activity with easily reduced substrates.[3] It forms spontaneously upon dissolution of *meso*- or *dl*-bi(3,5,5-trimethyl-2-oxomorpholin-3-yl) (*meso*- and *dl*-TM-3 dimers) in solvents ranging from hydrocarbons to water.[4,5] TM-3 exists in equilibrium with *meso*- and *dl*-TM-3 dimers in the absence of

† Also a member of The Cooperative Institute for Research in Environmental Sciences.

(1) Viehe, H. G.; Merényi, R.; Stella, L.; Janousek, Z. *Angew. Chem., Int. Ed. Engl.* **1979**, *18*, 917. Viehe, H. G.; Janousek, Z.; Merényi, R.; Stella, L. *Acc. Chem. Res.* **1985**, *12*, 148.

(2) Baldock, R. W.; Hudson, P.; Katritzky, A. R. *J. Chem. Soc., Perkin Trans. 1* **1974**, 1422.

(3) Burns, J. M.; Wharry, D. L.; Koch, T. H. *J. Am. Chem. Soc.* **1981**, *103*, 849.

0002-7863/92/1514-186$03.00/0